

A search for Low Surface Brightness galaxies in the near-infrared

III. Nançay H_I line observations

D. Monnier Ragaigne¹, W. van Driel¹, S.E. Schneider², C. Balkowski¹, and T.H. Jarrett³

¹ Observatoire de Paris, GEPI, CNRS UMR 8111 and Université Paris 7, 5 place Jules Janssen, F-92195 Meudon Cedex, France

e-mail: delphine.ragaigne@obspm.fr; wim.vandriel@obspm.fr; chantal.balkowski@obspm.fr

² University of Massachusetts, Astronomy Program, 536 LGRC, Amherst, MA 01003, U.S.A.

e-mail: schneide@messier.astro.umass.edu

³ IPAC, Caltech, MS 100-22, 770 South Wilson Ave., Pasadena, CA 91125, U.S.A.

e-mail: jarrett@ipac.caltech.edu

Received 5/3/2003; accepted 15/5/2003

Abstract. A total of 334 Low Surface Brightness galaxies detected in the 2MASS all-sky near-infrared survey have been observed in the 21 cm H_I line using the Nançay telescope. All have a K_s -band mean central surface brightness, measured within a 5'' radius, fainter than 18 mag arcsec⁻² and a K_s -band isophotal radius at the 20 mag arcsec⁻² level larger than 20''. We present global H_I line parameters for the 171 clearly detected objects and the 23 marginal detections, as well as upper limits for the undetected objects. The 171 clear detections comprise 50 previously uncatalogued objects and 41 objects with a PGC entry only.

Key words. Galaxies: distances and redshifts – Galaxies: general – Galaxies: ISM – Infrared: galaxies – Radio lines: galaxies

1. Introduction

The present paper is part of a series presenting the results of a multi-wavelength (near-infrared, 21-cm H_I line and optical) search for Low Surface Brightness (LSB) galaxies using the 2MASS all-sky near-infrared survey. For further details on the sample and other publications in this series, we refer to Monnier Ragaigne et al. (2003a, Paper I). H_I line observations made at Arecibo of a sample of a further 367 2MASS candidate LSB galaxies are presented in Paper II (Monnier Ragaigne et al. 2003b).

1.1. Low Surface Brightness galaxies

The brightness of the night sky acts as a filter in the selection of galaxies: when convolved with the true population of galaxies it gives the population of galaxies we observe. In the past few decades, observations of the local universe have shown the existence of LSB galaxies well below the surface brightness of the average previously catalogued galaxies. At present, the LSBs constitute the least well known fraction of galaxies: their number density and physical properties (luminosity, colours, dynamics) are still quite uncertain. This is mainly due to the

fundamental difficulty in identifying them in imaging surveys and in measuring their properties. In order to further investigate the properties of the LSB class of galaxies we selected a large sample of them from the 2MASS database, accessing a wavelength domain (the near-infrared) hitherto scarcely explored in the study of LSBs.

There is no unambiguous definition of LSB galaxies, although ones in common use are based on the mean surface brightness within an isophote or within the half-light radius, or on the extrapolated central surface brightness of the disc component alone after carrying out a disc-bulge decomposition. For 2MASS galaxies, we used the mean K_s -band magnitude within a fixed aperture to identify a sample of galaxies with relatively low infrared surface brightnesses. Because galaxies typically have $(B - K) \sim 3.5\text{--}4$ (see below) we selected galaxies in which the central surface brightness within a 5'' radius circular aperture was fainter than 18 mag arcsec⁻² in K_s . This criterion corresponds roughly to the disc-component definition of LSBs which have a blue central surface brightness $\mu_{B_0} > 22.0$ mag arcsec⁻².

LSBs have remarkable properties which distinguish them from high surface brightness spirals, notably:

- LSBs seem to constitute at least 50% of the total galaxy population in number in the local Universe,

which has strong implications for the faint end slope of the galaxy luminosity function, on the baryonic matter density and especially on galaxy formation scenarios (O'Neil & Bothun 2000).

- LSBs discs are among the less evolved objects in the local universe since they have a very low star formation rate (van der Hulst et al. 1993; van Zee et al. 1997; van den Hoek et al. 2000).
- LSBs are embedded in dark matter halos which are of lower density and more extended than the haloes around High Surface Brightness (HSB) galaxies, and they are strongly dominated by Dark Matter at all radii (e.g., de Blok et al. 1996; McGaugh et al. 2001)

The star formation history of LSBs has been the subject of recent debate. The LSBs best studied in the optical and in the near-infrared are blue (e.g., Bergvall et al. 1999), indicating a young mean stellar age and/or metallicity. Morphologically, most studied LSBs have discs, but little spiral structure. The current massive star formation rates in LSBs are an order of magnitude lower than those of HSBs (van Zee et al. 1997); H_I observations show that LSBs have high gas mass fractions, sometimes exceeding unity (Spitzak & Schneider 1998; McGaugh & de Blok 1997). All these observations are consistent with a scenario in which LSBs are relatively unevolved, low mass surface density, low metallicity systems with roughly constant star formation rate. However, this scenario has difficulty accommodating giant LSBs like Malin 1 (Bothun et al. 1987).

This study of infrared LSBs was also intended to investigate the possibility of the existence of a substantial population of red LSBs, like those reported by O'Neil et al. (1997b). Although the H_I study of O'Neil et al. (2000) indicated that some of them did not seem to follow the 'standard' Tully-Fisher relation, appearing to be severely underluminous for their total mass, observations by Chung et al. (2002) indicate that their rotational properties were mismeasured due to confusion with neighbouring galaxies. An infrared-selected sample should allow us to identify whether there is a significant population of very red LSBs.

In the present paper results of 21-cm H_I line observations made at Nançay is given, whereas a description of the 2MASS LSB galaxy sample selection is given in Paper I, H_I observations made at Arecibo are presented in Paper II, optical BVRI CCD surface photometry of a sub-sample of 35 galaxies will be presented in Paper IV (Monnier Ragaigne et al. 2003d), an analysis of the full data set will be presented in paper V in the series, and models of the star formation history of these, and other, samples of LSB galaxies are presented in Boissier et al. (2003).

1.2. The 2MASS all-sky near-infrared survey

The Two Micron All Sky Survey, 2MASS, has imaged the entire celestial sphere in the near-infrared *J* (1.25 μ m), *H*

(1.65 μ m) and *K_s* (2.16 μ m) bands from two dedicated, identical 1.3-meter telescopes. The 2MASS data have a 95% completeness level in *J*, *H* and *K_s* of 15.1, 14.3 and 13.5 mag, respectively, for 'normal' galaxies (Jarrett et al. 2000; for LSB and blue objects the completeness limits are not yet known). The Extended Source Catalog (XSC) will consist of more than 1.4 million galaxies brighter than 14th mag at *K_s* with angular diameters greater than \sim 6''. The photometry includes accurate PSF-derived measures and a variety of circular and elliptical aperture measures, fully characterizing both point-like and extended objects. The position centroids have an astrometric accuracy better than \sim 0''.5. In addition to tabular information, 2MASS archives full-resolution images for each extended object, enabling detailed comparison with other imaging surveys. Initial results for galaxies detected by 2MASS, detailing their properties and detection into the Zone of Avoidance (ZoA), are described in several publications (Schneider et al. 1997; Jarrett et al. 2000a, 2000b; Hurt et al. 2000).

Though relatively less deep than some of the dedicated optical imaging surveys made of LSB galaxies over limited areas of the sky, the 2MASS survey allows the detection of LSBs with a central surface brightness in the *K_s* band of \sim 18-20 mag arcsec⁻², corresponding to about \sim 22-24 mag arcsec⁻² in *B*, extending over the entire sky. The near-infrared data will be less susceptible than optical surveys to the effects of extinction due to dust, both Galactic and internal to the galaxies.

The selection of the sample of 2MASS near-infrared selected LSB galaxies observed in H_I at Nançay is described in Section 2, the observations and the data reduction are presented in Section 3, and the results in Section 4. A brief discussion of the results is given in Section 5 and the conclusions are presented in Section 6.

2. Sample selection

We have selected 2MASS LSB galaxies using the following two galaxy search routines. For a more complete description of the selection procedures we refer to Paper I. The selected LSB objects lie outside the ZoA ($|b|>10^\circ$).

- The first is aimed at selecting relatively high signal-to-noise low central surface brightness (LCSB) galaxies, with a mean central *K_s* surface brightness in the inner 5'' radius of $K_5 \geq 18$ mag arcsec⁻², among the extended sources picked out from the survey data by the standard 2MASS algorithms (Jarrett et al. 2000). All objects observed in H_I at Nançay have a 20 mag arcsec⁻² *K_s*-band isophotal radius $r_{K_{20}}$ larger than 20'', i.e., they belong to our sample of "Large" sources (see Paper I).

- The second is aimed at finding lower signal-to-noise LSB galaxies among those sources which were not recognized as such during the standard extended source selection described above. This requires masking all sources detected by the former method and spatially smoothing the remaining data. These sources are referred to as the "Faint" sample, see Paper I.

In order to decide which of these 2MASS sources really are LSB galaxies, additional data were used from online databases such as NED (NASA Extragalactic Database) [<http://nedwww.ipac.caltech.edu>], LEDA (Lyon-Meudon Extragalactic Database) – recently incorporated in HyperLeda [<http://www-obs.univ-lyon1.fr/hypercat/>] – and Aladin of the Centre de Données astronomiques de Strasbourg (CDS) [<http://aladin.u-strasbg.fr>], and Digital Sky Survey (DSS) images were inspected. Using this selection procedure, a total of 3,800 candidate 2MASS LSB galaxies were found.

The source selection for our survey was made with the 2MASS working database available in late 1999, when work on it was still in full progress. The 229 Large sources we observed at Nançay contain only 12 that are not found in the subsequent, more reliable, 2MASS public data releases (see paper I for details), 6 of which were detected by us in H_I (L125O, L191O, L192O, L270O, L668O and L734O) and 6 that were not (L147N, L328O, L649P, L673O, L761N and L791). Their names have been put in parentheses in the Tables. The sample also contains 19 Faint sources, out of the 25 observed at Nançay, that are not found in subsequent public data releases. This high percentage is not surprising, however, considering they were detected by a dedicated LSB galaxy search method and that they were not included in the working database. Thirteen of these were detected (see Table 4) and 6 were not (see Table 7).

Due to constraints in the useable declination range of the instrument, the area of the sky observed at Nançay for our survey ranges from -39° to 60° in declination, and excludes the declination range we observed at Arecibo, i.e. 0° to $+39^\circ$. Within the chosen area we selected for observation, in order of decreasing priority: (1) all objects with known velocity, and (2) objects without known velocity, whether previously catalogued or not.

3. Observations and data reduction

3.1. Observations

The Nançay decimetric radio telescope, a meridian transit-type instrument of the Kraus/Ohio State design, consists of a fixed spherical mirror (300 m long and 35 m high), a tiltable flat mirror (200×40 m), and a focal carriage moving along a curved rail track. Sources on the celestial equator can be tracked for about 60 minutes. The telescope's collecting area is about 7000 m^2 (equivalent to a 94-m diameter parabolic dish). Due to the E-W elongated shape of the mirrors, some of the instrument's characteristics depend on the declination at which one observes. At 21-cm wavelength the telescope's half-power beam width (HPBW) is $3.5'$ in right ascension, independent of declination, while in the North-South direction it is $23'$ for declinations up to $\sim 20^\circ$, rising to $25'$ at $\delta = 40^\circ$ and to $29'$ at $\delta = 60^\circ$, the northern limit of the survey (see also Matthews & van Driel 2000). The instrument's effective collecting area and, consequently, its gain, follow the same

geometric effect, decreasing correspondingly with declination. All observations for our project were made after a major renovation of the instrument's focal system (e.g., van Driel et al. 1997), which resulted in a typical system temperature of 35 K.

The observations were made in the period July 2000–June 2002, using a total of about 1500 hours of telescope time. We obtained our observations in total power (position-switching) mode using consecutive pairs of 40 seconds ON and 40 seconds off-source integrations. Off-source integrations were taken at a position about $20'$ E of the target position. Different autocorrelator modes were used for the observation of sources with previously known radial velocities and for velocity searches of objects of unknown redshift.

For objects of known redshift, the autocorrelator was divided into 1 pair of cross-polarized receiver banks, each with 4096 channels and a 25 MHz bandpass, resulting in a channel spacing of 1.3 km s^{-1} . The centre frequencies of the 2 banks were tuned to the redshifted H_I line frequency of the target source. These spectra were boxcar smoothed to a channel separation of 17.1 km s^{-1} during the data reduction in order to increase signal-to-noise.

For objects without a known redshift, the autocorrelator was divided into 1 pair of cross-polarized receiver banks, each with 4096 channels and a 50 MHz bandpass, resulting in a channel spacing of 2.6 km s^{-1} . The centre frequencies of the 2 banks were tuned to 5600 km s^{-1} , for a velocity search in the ~ 500 to $10,500 \text{ km s}^{-1}$ range (hereafter referred to as a low-velocity search) and to $15,000 \text{ km s}^{-1}$, for a velocity search in the ~ 9500 to $20,500 \text{ km s}^{-1}$ range for the ‘high-velocity searches’. These spectra were boxcar smoothed to a channel separation of 15.7 km s^{-1} during the data reduction.

Flux calibration, i.e., the conversion of observed system temperatures to flux densities in mJy, is determined for the Nançay telescope through regular measurements of a cold load calibrator and periodic monitoring of strong continuum sources by the Nançay staff. Standard calibration procedures include correction for the abovementioned declination-dependent gain variations of the telescope (e.g., Fouqué et al. 1990). We observed a number of calibrator galaxies throughout our observing runs, see Section 5.

3.2. Data reduction

The first steps in the data reduction were made using software developed by the Nançay staff (NAPS, SIR program packages). With this software we averaged the two receiver polarizations, and applied a declination-dependent conversion factor to convert from units of system temperature to flux density in mJy.

Further data analysis was performed using Supermongo routines developed by one of us (SES). With these we subtracted baselines (generally third order polynomials were fitted), excluding those velocity ranges

with H_I line emission or radio frequency interference (RFI). Once the baselines were subtracted, the radial velocities were corrected to the heliocentric system, according to the conventional optical definition ($V = c(\lambda - \lambda_0)/\lambda_0$) and the central line velocity, line widths at, respectively, the 50% and 20% level of peak maximum (Lewis 1983), the integrated flux of the H_I profiles, as well as the rms noise of the spectra were determined. All data were boxcar smoothed to a velocity resolution of 15.7 km s⁻¹ (velocity search) and 17.1 km s⁻¹ (known velocity) for further analysis.

3.2.1. RFI mitigation

As a consequence of their high sensitivity, radio astronomy telescopes are vulnerable to radio frequency interference (RFI), with signal strengths usually greatly exceeding those of the weak celestial radio sources being observed. Broad-band RFI raises the noise level of the observations, while narrow-band RFI may mimic spectral lines, like the H_I lines from galaxies that were searched for in the present study.

In a regulatory sense, for 21cm line observations, it should be noted that in the ITU-R Radio Regulations (2001), with which all users of the radio spectrum are obliged to comply, astronomical H_I line observations are only protected from “all emissions” out to a redshift of about 4300 km s⁻¹, while for observations out to $\sim 19,000$ km s⁻¹ “[national frequency] administrations are urged to take all practicable steps to protect the radio astronomy service from harmful interference”. These provisions for protection from RFI clearly cannot guarantee a completely interference-free environment for the kind of survey we performed.

At present no universal RFI mitigation method exists for radio astronomy observations (e.g., Fridman & Baan 2001). In order to minimize the effect of RFI in our observations we used an off-line RFI mitigation program, which is part of the standard Nançay NAPS software package. The different steps applied to the individual 40 second integration spectra within a cycle of consecutive spectra of a particular object are as follows:

First, the average of all OFF spectra in the cycle is subtracted from each individual ON spectrum, and then for each resulting individual spectrum the average signal strength and its rms variation is determined, after rejection of 25% of the highest and 25% of the lowest signal strengths. In each individual spectrum the channels with signal strengths deviating by more than $\pm N\sigma$ from the average are flagged, and their signal strengths replaced by a linear interpolation between neighbouring clean channels. The cut-off level was set to 10σ .

Then the average of all cleaned ON spectra in the cycle is subtracted from each individual OFF spectrum. In analogy with the first step, in each resulting individual spectrum the channels with signal strengths exceeding $\pm N\sigma$

from the average are replaced by linear interpolation. This results in cleaned individual OFF spectra.

Finally, the first step is repeated on the individual ON spectra, but this time using the cleaned OFF spectrum resulting from the second step.

Nevertheless, no RFI mitigation technique can simply eliminate all interference (certainly not without the risk of removing part of the line emission that is being searched for), and the detections in the following radial velocity ranges, where the strongest RFI signals occur, should be considered with due care: RFI occurred frequently around 4200, 8250, 12,500 and 17,200 km s⁻¹, regularly around 9000 and 11,700 km s⁻¹, and occasionally around 2000, 9400 and 10,500 km s⁻¹.

4. Results

Our global Nançay H_I data for the observed sample, together with their global near-infrared and optical data, are listed in Table 3 for detected objects, in Table 4 for marginal detections and in Table 5 for undetected objects. The H_I spectra of the detected galaxies are shown in Figure 1; for information on cases where 2 line profiles were detected in the same spectrum, which are designated by ‘a’ and ‘b’ after the 2MASS source name, see Sect. 4.5. For marginal detections, the H_I spectra are shown in Figure 2.

A description of all parameters listed in the Tables is given below in Sections 4.1-4.4. The near-infrared data listed were taken from the 2MASS catalogue and the optical data were taken from the online NED and LEDA databases, as indicated.

The distribution of the integrated line fluxes and FWHM’s of the clear and marginal detections is shown in Figure 3. Also plotted in this Figure is a straight line indicating the 3σ detection limit for a 250 km s⁻¹ wide, flat-topped spectral line, based on the average rms noise level of the data. The data quality and the rms noise in the observations is not very uniform in general, not even for the spectra in which detections were made, resulting in the dispersion among the weakest clear and marginal detections.

4.1. Names, positions and distances

- Number: we have divided the selected 2MASS sources according to two criteria: size and algorithm. This division is indicated by two characters in the galaxy designations which we will use throughout this series: ‘L’ indicates that all objects we observed at Nançay are “Large” object with an isophotal K_s -band radius r_{K20} (see Sect. 4.2) larger than 20'' (note that no “Small” sources, with a radius between 10'' and 20'', were observed at Nançay) and an ‘F’ a galaxy selected using the LCSB source processor, while following the source number an ‘O’ indicates a previously catalogued object, a ‘P’ one with a PGC entry only and an ‘N’ a previously uncatalogued one.

- Identifications: for each of the 2MASS sources we queried the NED and LEDA databases for a cross-identification of its position with other catalogues. For previously catalogued objects we list the most commonly used identification besides the 2MASS identification;
- Positions: the listed right ascensions and declinations are the catalogued 2MASS source centre positions, for epoch J2000.0. These were used as the pointing centres for the H I observations;
- Distances: for each detected galaxy, a distance D was calculated using radial H I velocities corrected to the Galactic Standard of Rest, following the procedure given in the RC3 (and used in LEDA), and assuming a Hubble constant of $H_0=75 \text{ km s}^{-1} \text{ Mpc}^{-1}$.

4.2. Near-infrared data

- K_{20} is the total magnitude measured within the $r_{K_{20}}$ isophotal aperture (see below);
- $J - K$ is the $(J - K)_{20}$ near-infrared colour, based on magnitudes measured in the J and K_s bands within their respective isophotal semi-major axes at the 20 mag arcsec $^{-2}$ level;
- μ_{K5} is the mean central surface brightness (in mag arcsec $^{-2}$) measured within a radius of 5 arcsec around the source's centre;
- b/a is the infrared axis ratio determined from an ellipse fit to the co-addition of the J -, H -, and K_s -band images. The fit is carried out at the 3- σ isophotal level relative to the background noise in each image. The 2MASS F (LCSB sources) sample was not measured in this way because of the low signal-to-noise levels of the emission;
- $r_{K_{20}}$ is the fiducial aperture (in arcsec) in K band. Essentially, it is the aperture size for a surface brightness of 20 mag arcsec $^{-2}$ in K band;
- L_K is the absolute magnitude in the K band (in $L_{\odot,K}$), calculated using an absolute solar K -band magnitude of 3.33 (Allen 1973).

4.3. Optical data

- Type is the morphological type, as listed in NED;
- V_{opt} is the mean heliocentric radial velocity (in km s $^{-1}$), as listed in LEDA;
- D_{25} is the isophotal B -band diameter (in units of arcmin) measured at a surface brightness level of 25 mag arcsec $^{-2}$, as listed in LEDA;
- B_{T_c} is the total apparent B -band magnitude reduced to the RC3 system (de Vaucouleurs et al. 1991) and corrected for galactic extinction, inclination and redshift effects (see Paturel et al. 1997, and references therein), as listed in LEDA;
- $\mu_{B_{25}}$ is the mean B -band surface brightness (in mag arcsec $^{-2}$) within the 25 mag arcsec $^{-2}$ isophote, as listed in LEDA;
- L_B is the absolute magnitude in the B band (in $L_{\odot,B}$), calculated using the B_{T_c} magnitude and an absolute solar

magnitude in the B band of 5.48 (Allen 1973), as listed in LEDA.

4.4. H I data

The global H I line parameters are directly measured values; no corrections have been applied to them for, e.g., instrumental resolution or cosmological stretching (e.g., Matthews et al. 2001)

- rms is the rms noise level in a spectrum (in mJy);
 - I_{HI} is the integrated line flux (in Jy km s $^{-1}$). The upper limits listed are 3 σ values for flat-topped profiles with a width of 250 km s $^{-1}$, a representative value for the galaxies detected;
 - V_{HI} is the heliocentric central radial velocity of a line profile (in km s $^{-1}$), in the optical convention. We estimated the uncertainty, $\sigma_{V_{HI}}$ (in km s $^{-1}$), in V_{HI} following Fouqué et al. (1990), as
- $$\sigma_{V_{HI}} = 4R^{0.5}P_W^{0.5}X^{-1} \quad (1)$$
- where R is the instrumental resolution ($\sim 17 \text{ km s}^{-1}$, see Section 3.1), $P_W=(W_{20}-W_{50})/2$ (in km s $^{-1}$) and X is the signal-to-noise ratio of a spectrum, which we defined as the ratio of the peak flux density and the rms noise;
- V_0 is the H I radial velocity (in km s $^{-1}$) corrected to the Galactic Standard of Rest, following the RC3;
 - W_{50} and W_{20} are the velocity widths (in km/s) at 50% and 20% of peak maximum (km/s). According to Fouqué et al. (1990), the uncertainty in the line widths is $2\sigma_{V_{HI}}$ (see above) for W_{50} and $3\sigma_{V_{HI}}$ for W_{20} .
 - M_{HI} is the total H I mass (in M_{\odot}), $M_{HI}=2.356 \cdot 10^5 D^2 I_{HI}$;
 - M_{HI}/L_B is the ratio of the total H I mass to the B -band luminosity (in $M_{\odot}/L_{\odot,B}$);
 - M_{HI}/L_K is the ratio of the total H I mass to the K_s -band luminosity (in $M_{\odot}/L_{\odot,K}$).

4.5. Notes on individual galaxies

In order to identify possible confused sources in our H I observations, we first inspected DSS images over a region of $12' \times 36'$ ($\alpha \times \delta$) centred on the 2MASS position of each clearly or marginally detected source. In case galaxies were noted that might give rise to confusion with the H I profile of the target galaxy, we queried the NED and LEDA databases for data on the objects. The data listed here were preferentially taken from the mean values listed in LEDA. The global H I line parameters of galaxies reported as detected in the literature are listed in Table 2.

L60: 2MASXJ00140398-2310555 = NGC 45: the 2MASS source is a bright H II region in the outer disc of this large ($D_{25}=7.4'$) spiral, whose E-W extent far exceeds the 3.6 Nançay HPBW. This explains why our integrated H I line flux of 66 Jy km s $^{-1}$, is much lower than the mean literature value of 245 Jy km s $^{-1}$ (LEDA), which was measured with larger telescope beams covering the entire galaxy.

L29O: 2MASXIJ0041576-325810 = ESO 351-G2: our H_I detection ($V_{HI}=9560$ km s⁻¹, $W_{50}=193$: km s⁻¹) appears to have its high-velocity edge reduced by negative RFI, and it may be confused by a nearby galaxy. The target galaxy ($V_{opt}=9618\pm49$ km s⁻¹, $B_T=15.27$, $D_{25}=0.9$), has an edge-on companion at 1'1 separation, MCG-6-2-24 ($V_{opt}=9525\pm60$ km s⁻¹, $B_T=16.55$, $D_{25}=0.6$); both are classified as Sc spirals. Both galaxies have a systemic velocity corresponding to the H_I velocity, within the errors, but the companion is 1.3 mag weaker.

L57O: 2MASXJ01190447-0008190 = UGC 847: our H_I detection ($V_{HI}=5238$ km s⁻¹, $W_{50}=271$ km s⁻¹) may be slightly confused by a nearby galaxy. The edge-on target galaxy, ($V_{opt}=5218\pm60$ km s⁻¹, $B_T=16.29$, $D_{25}=1.4$, Scd) has a companion 3'5 East of it, i.e. well outside the telescope's HPBW, PGC 212709 ($V_{opt}=5173\pm22$ km s⁻¹ [Sloan Survey], $B_T=16.27$, $D_{25}=0.6$).

L59O: 2MASXJ01222287-3636297 = ESO 352-G58: our H_I profile may in principle be confused, as at only 0'5 from the centre of the target galaxy, ($B_T=15.82$, $D_{25}=1.2$, Sbc), lies the much smaller Irr galaxy PGC 634708 ($B_T=17.75$, $D_{25}=0.35$). Neither has a known optical redshift, however.

L70O: 2MASXJ01430297-3411143 = IC 1722: though our H_I profile looks rather complex, with $V_{HI}=3911$ km s⁻¹ and $W_{50}=515$ km s⁻¹, it does not seem likely it is confused with two nearby early-type galaxies. The target galaxy ($V_{opt}=4082\pm35$ km s⁻¹, $B_T=14.68$, $D_{25}=1.5$, SBbc), is highly inclined, as are nearby IC 1724 ($V_{opt}=3836\pm51$ km s⁻¹, $B_T=14.53$, $D_{25}=1.2$, S0), 3'6 to the south, and ESO 353-G36 ($V_{opt}=3774\pm137$ km s⁻¹, $B_T=15.11$, $D_{25}=1.0$, SO-a), 3'4 to the east, outside the HPBW. Although the systemic velocities of the latter two objects are closer to the H_I velocity, they are both classified as lenticulars and therefore not expected to be gas-rich.

L86O: 2MASXJ01590735-0308587 = MCG -1-6-13: 1'1 east of the target galaxy MCG -1-6-13 ($V_{opt}=5342\pm42$ km s⁻¹, $B_T=14.71$, $D_{25}=1.0$, Irr), lies an Sa spiral of unknown velocity, KUG 0156-033 ($B_T=15.22$, $D_{25}=0.55$, Sa).

L117O: 2MASXJ02284546-1030501 = NGC 948: our H_I profile of this object ($V_{HI}=4758$ km s⁻¹, $W_{50}=168$ km s⁻¹, $I_{HI}=5.0$ Jy km s⁻¹) is probably confused with that of its larger neighbour NGC 945. At 2'5 from the target galaxy ($V_{opt}=4511\pm43$ km s⁻¹, $B_T=14.38$, $D_{25}=1.2$, SBC), lies the larger spiral NGC 945 ($V_{opt}=4484\pm60$ km s⁻¹, $B_T=12.89$, $D_{25}=2.2$, SBC). At Nançay Theureau et al. (1998) detected NGC 945 ($V_{HI}=4482$ km s⁻¹, $W_{50}=179$ km s⁻¹, $I_{HI}=4.0$ Jy km s⁻¹), while at Arecibo Haynes et al. (1999) detected NGC 948 ($W_{50}=181$ km s⁻¹, $I_{HI}=6.0$ Jy km s⁻¹). The E-W HPBW of the two telescopes is quite similar, 3'6, and serious confusion is inevitable between the line signal of both galaxies, whose centres are separated by 2'5.

(L125O): 2MASXi J0235204+405522 = NGC 980: This object is classified as an S0 and therefore unlikely to be detectable in H_I, and our H_I spectrum ($V_{HI}=5744$

km s⁻¹, $W_{50}=592$ km s⁻¹, $I_{HI}=4.0$ Jy km s⁻¹) is confused by nearby galaxies. Within the same telescope beam as the target object ($V_{opt}=5796\pm42$ km s⁻¹, $B_T=14.27$, $D_{25}=1.7$), lies the Sa spiral NGC 982 ($V_{opt}=5845\pm52$ km s⁻¹, $B_T=13.16$, $D_{25}=1.5$) at 3'3, the Sd spiral UGC 2068 ($B_T=17.68$, $D_{25}=0.75$) at 2'1 and the SBb spiral MCG +7-6-40 ($B_T=17.96$, $D_{25}=0.35$) at 4'2 distance; the latter two do not have a known redshift. NGC 980 was detected at Arecibo ($V_{HI}=5757$ km s⁻¹, $W_{50}=702$ km s⁻¹, $I_{HI}=8.2$ Jy km s⁻¹; Haynes et al. 1988), NGC 982 also at Arecibo ($V_{HI}=5737$ km s⁻¹, $W_{50}=568$ km s⁻¹, $I_{HI}=7.0$ Jy km s⁻¹; Magri 1994) and UGC 2068 at Nançay ($V_{HI}=5740$ km s⁻¹; Theureau et al. 1998). Seen the similar optical redshifts of NGC 980 and 982 and their proximity all published H_I profiles of these objects must be confused.

L161O: 2MASXIJ0306290-094332 = IC 1880: it is not clear to which galaxy our H_I detection ($V_{HI}=3935$ km s⁻¹, $W_{50}=144$ km s⁻¹, $I_{HI}=9.2$ Jy km s⁻¹) is due. The target galaxy is a lenticular at $V_{opt}=10.224\pm42$ km s⁻¹. There is one other galaxy in the beam, of unknown redshift, PGC 135017 ($B_T=16$, $D_{25}=0.7$, Sc) and another outside the HPBW, NGC 1208 ($V_{opt}=4518\pm53$ km s⁻¹, $B_T=13.31$, $D_{25}=1.9$), which has a too high redshift and is classified as SO/a. Only a weak H_I line was detected towards NGC 1208 at Nançay by Theureau et al. (1998): $V_{HI}=4356$ km s⁻¹, $W_{50}=259$ km s⁻¹, $I_{HI}=0.5$ Jy km s⁻¹.

L184O 2MASXJ03234832+4033485 = UGC 2708: it is not clear if the marginal H_I detection ($V_{HI}=8582$: km s⁻¹, $W_{50}=295$: km s⁻¹, $I_{HI}=6.5$: Jy km s⁻¹) is (mainly) due to residual RFI from the GPS L3 band centered on 8250 km s⁻¹ (see Section 3.2.1), or to a galaxy. It is ~ 3200 km s⁻¹ higher than the optical redshift of the target galaxy, 5390 ± 51 km s⁻¹. Furthermore the galaxy has been classified as SB0 and is therefore unlikely to be detectable. There are no likely candidates for confusion in the vicinity. We therefore consider this a tentative detection only.

L203O: 2MASXJ03404154-2239041 = ESO 482-G31: our narrow H_I detection ($V_{HI}=1683$ km s⁻¹, $W_{50}=60$ km s⁻¹, $I_{HI}=0.5$ Jy km s⁻¹) may be due to a nearby galaxy. The target galaxy ($V_{opt}=1629\pm43$ km s⁻¹, $B_T=15.27$, $D_{25}=0.9$) is classified as an S0. At the edge of the beam lies the much larger NGC 1415 ($V_{opt}=1549\pm47$ km s⁻¹, $B_T=12.77$, $D_{25}=3.3$). Though classified as S0/a, it has quite a strong H_I line as detected, respectively, at Nançay (Balkowski 1979) and Effelsberg (Huchtmeier 1982): mean values $V_{HI}=1585$ km s⁻¹, $W_{50}=322$ km s⁻¹ and $I_{HI}=8.3$ Jy km s⁻¹.

L237O: 2MASXJ04294085-2724313 = NGC 1592: This Irregular object appears to be a merger or a very close, interacting pair of galaxies.

L249O: 2MASXIJ0443334-274006 = ESO 421-G13: our H_I spectrum shows two peaks, at $V_{HI}=5353$ and $10,457$ km s⁻¹, respectively. The target galaxy ($B_T=15.3$, $D_{25}=1.2$, Sbc) does not have a known optical redshift; there is no other candidate for confusion within the beam

in the search area. Seen its size and magnitude, an association with the 5353 km s^{-1} profile seems the most likely.

L255O: 2MASXJ04511837-0557379 = MCG -01-13-021: One nearby galaxy, 2MASXi J0451123-060013, lies within the beam, while two others lie on the edge of the beam: MCG -01-13-020 ($B_T=15.29$, $D_{25}=1'0$) and 2MASXi J0451085-060321. Like the target galaxy ($B_T=15.23$, $D_{25}=1'5$, Sc), none of these have a known redshift.

L256O: 2MASXJ04551547-1209275 = MCG -2-13-23: It is not clear to which of the two galaxies in the telescope beam galaxy our detection ($V_{HI}=4862 \text{ km s}^{-1}$, $W_{50}=231 \text{ km s}^{-1}$, $I_{HI}=4.4 \text{ Jy km s}^{-1}$) is due, as the target galaxy has an optical redshift of $17,881 \pm 60 \text{ km s}^{-1}$ (Huchra et al. 1993), which is far outside our velocity search range, while the other galaxy in the beam, MCG -2-13-22, is an S0 with $V_{opt}=8133 \pm 60 \text{ km s}^{-1}$. The observed line signal may be spurious and due imperfectly filtered out RFI.

L272O: 2MASXJ05153881-2242320 = ESO 486-G40 : It seems unlikely that our detection is confused by the one magnitude weaker AM 0513-224, of unknown redshift, at the edge of the beam. Our H_I redshift of the target galaxy, 5796 km s^{-1} , corresponds to its optical value of $5779 \pm 42 \text{ km s}^{-1}$.

L297O: 2MASXJ06131885+5306445 = UGC 3421: It is not clear if our H_I detection of the target galaxy ($D_{25}=0'9$, Sd) may be confused by a galaxy at the edge of the beam (at $3'3$ EW separation), UGC 3424 ($B_T=16.24$, $D_{25}=1'2$, Irr), as neither has a published redshift.

L302O: 2MASXJ06243891-2235497 = ESO 489-G50: The target galaxy ($V_{opt}=2892 \text{ km s}^{-1}$, $B_T=15.79$, $D_{25}=1'4$), is classified as S0-a and therefore unlikely to be gas-rich. Our H_I detection ($V_{HI}=2713 \text{ km s}^{-1}$, $W_{50}=316 \text{ km s}^{-1}$, $I_{HI}=9.8 \text{ Jy km s}^{-1}$) appears due to a large galaxy at the edge of the beam, $14'4$ south of the target galaxy, NGC 2223 ($V_{opt}=2690 \pm 61 \text{ km s}^{-1}$, $B_T=12.51$, $D_{25}=2'9$, SBc), whose mean H_I profile parameters are $V_{HI}=2721 \text{ km s}^{-1}$, $W_{50}=300 \text{ km s}^{-1}$ and $I_{HI}=26 \text{ Jy km s}^{-1}$ (Bottinelli et al. 1982; Fisher & Tully 1981; Staveley-Smith & Davies 1987).

L336O: 2MASXIJ0819021+211122 = UGC 4329: the redshift of our H_I detection ($V_{HI}=4079 \text{ km s}^{-1}$, $W_{50}=222 \text{ km s}^{-1}$, $I_{HI}=6.8 \text{ Jy km s}^{-1}$) is in agreement with the $V_{opt}=4144 \pm 73 \text{ km s}^{-1}$, and the spectrum is unlikely to be confused by the 4 galaxies that lie at the edge of the beam (CGCG 119-043, CGCG 119-053, NGC 2556 and NGC 2557) as they all have redshifts in the range of 4460 - 4860 km s^{-1} . Its line parameters agree with the published mean values of $V_{HI}=4097 \text{ km s}^{-1}$, $W_{50}=223 \text{ km s}^{-1}$ and $I_{HI}=8.7 \text{ Jy km s}^{-1}$ (Bicay & Giovanelli 1986; Bothun et al. 1985; Lewis 1983; Lewis et al 1985; Rosenberg & Schneider 2000; Schommer et al. 1981; Tifft & Cocco 1988).

L345O: 2MASXJ08325749-2254031 = ESO 495-G17: our H_I detection ($V_{HI}=1416 \text{ km s}^{-1}$, $W_{50}=205 \text{ km s}^{-1}$, $I_{HI}=3.2 \text{ Jy km s}^{-1}$) may be due to gas in the outer disc of the nearby large spiral NGC 2613. Another Nançay spectrum (Chamaraux et al. 1999) of our target galaxy

($B_T=14.76$, $D_{25}=1'4$, Sb), of unknown redshift, shows $W_{50}=178 \text{ km s}^{-1}$ and $I_{HI}=3.9 \text{ Jy km s}^{-1}$. Although the centre of NGC 2613 ($V_{opt}=1599 \pm 88 \text{ km s}^{-1}$, $B_T=11.15$, $D_{25}=7'0$) lies 7.3 SE of that of the target galaxy, its diameter is large enough to cause confusion. H_I observations of NGC 2613 (Bottinelli et al. 1982; Fisher & Tully 1981; Reif et al. 1982; Staveley-Smith & Davies 1987) show mean parameters of $V_{HI}=1678 \text{ km s}^{-1}$, $W_{50}=599 \text{ km s}^{-1}$ and $I_{HI}=83 \text{ Jy km s}^{-1}$.

L358O: 2MASXJ08565629-2031383 = ESO 563-G34: our narrow H_I profile (($V_{HI}=2616 \text{ km s}^{-1}$, $W_{50}=97 \text{ km s}^{-1}$, $I_{HI}=4.4 \text{ Jy km s}^{-1}$) of the target galaxy ($V_{opt}=2558 \pm 60 \text{ km s}^{-1}$, $B_T=14.32$, $D_{25}=1'2$, Sab) does not appear to be confused by a galaxy on the edge of the beam, at $\sim 3'$ E-W separation, ESO 563-G36 ($V_{opt}=2656 \pm 50 \text{ km s}^{-1}$, $B_T=13.88$, $D_{25}=1'4$, Sab).

L360O: 2MASXJ09001445+3543527 = NGC 2719: Confused H_I spectrum. The target galaxy ($V_{opt}=3172 \pm 46 \text{ km s}^{-1}$, $B_T=13.65$, $D_{25}=1'2$, Irr), forms a close pair ($0'5$ separation) with NGC 2719A ($V_{opt}=3069 \pm 43 \text{ km s}^{-1}$, $B_T=14.50$, $D_{25}=0'55$, Irr). Surprisingly, our H_I detection ($V_{HI}=3043 \text{ km s}^{-1}$, $W_{50}=215 \text{ km s}^{-1}$, $I_{HI}=9.3 \text{ Jy km s}^{-1}$) has a 114 km s^{-1} lower central velocity and a two times smaller integrated line flux than the Arecio profile of Bicay & Giovanelli (1986), with $V_{HI}=3157 \text{ km s}^{-1}$, $W_{50}=231 \text{ km s}^{-1}$ and $I_{HI}=17.9 \text{ Jy km s}^{-1}$, which also includes both galaxies.

L371O: 2MASXIJ0917317+415932 = NGC 2799: our H_I profile is confused, as there are two other sizeable galaxies of similar redshift in the beam of the target galaxy ($V_{opt}=1860 \pm 68 \text{ km s}^{-1}$, $B_T=13.98$, $D_{25}=1'8$, SBd): NGC 2798 ($V_{opt}=1735 \pm 67 \text{ km s}^{-1}$, $B_T=14.92$, $D_{25}=2'7$, SBa) and UGC 4904 ($V_{opt}=1644 \pm 60 \text{ km s}^{-1}$, $B_T=15.21$, $D_{25}=1'0$, SBbc). The E-W separation between NGC 2799/98 is $1'6$, i.e. only about half the Nançay HPBW. Our H_I profile has $V_{HI}=1616 \text{ km s}^{-1}$, $W_{50}=159 \text{ km s}^{-1}$ and $I_{HI}=9.1 \text{ Jy km s}^{-1}$, while the Nançay profile of NGC 2799 from Bottinelli et al. (1982) has $V_{HI}=1755 \text{ km s}^{-1}$, $W_{50}=340 \text{ km s}^{-1}$ and $I_{HI}=11.1 \text{ Jy km s}^{-1}$ and a Nançay profile of NGC 2798 (Bottinelli et al. 1980) has $V_{HI}=1726 \text{ km s}^{-1}$, $W_{50}=313 \text{ km s}^{-1}$ and $I_{HI}=11.5 \text{ Jy km s}^{-1}$. Our profile has a $\sim 125 \text{ km s}^{-1}$ lower central velocity and a two times smaller W_{50} . Profiles that include the three above-mentioned galaxies were published by Huchtmeier (1982) and Peterson & Shostak (1974).

(F26O) = MCG -1-25-33: our H_I profile is probably confused, since there is a pair of galaxies, of unknown redshift, of similar size in the beam of the target galaxy ($B_T=14.48$, $D_{25}=1'3$, SBcd): UGC A 173 ($V_{opt}=1875 \pm 97 \text{ km s}^{-1}$, $B_T=14.63$, $D_{25}=1'3$, SBd) and UGC A 174 ($B_T=14.85$, $D_{25}=1'3$, SBm). Our H_I profile ($V_{HI}=1883 \text{ km s}^{-1}$, $W_{50}=118 \text{ km s}^{-1}$, $I_{HI}=11.0 \text{ Jy km s}^{-1}$) agrees with the Richter & Huchtmeier (1987) Effelsberg profile of UGC A 173 ($V_{HI}=1867 \text{ km s}^{-1}$, $W_{50}=189 \text{ km s}^{-1}$, $I_{HI}=12.7 \text{ Jy km s}^{-1}$), which includes all three objects.

L392O: 2MASXJ09450315-0429475 = FGC 936: there are two galaxies, both of unknown redshift, with only $0'6$ separation at the centre of the beam, FGC 936

($B_T=16.6$, $D_{25}=0.9$, Sc) and 2MASXi J0945014-042919 (=PGC 1057506), with $B_T=16.45$ and $D_{25}=0.5$). While in NED the position of our 2MASS source coincides exactly with that of FGC 936, in LEDA it coincides exactly with that of the other galaxy. As the LEDA positions all have an accuracy of $10''$, significantly better than that from the FGC (Karachentsev et al. 1999), we adopted the latter association.

L403O: 2MASXJ10144367-2048367 = ESO 567-G28: our H_I profile ($V_{HI}=3705$ km s $^{-1}$, $W_{50}=208$ km s $^{-1}$, $I_{HI}=2.9$ Jy km s $^{-1}$) may in principle be confused. At about the HPBW level of our beam, pointed at the target galaxy ($B_T=15.43$, $D_{25}=1.2$, Sbc) lie two galaxies, also of unknown redshift: ESO 567-G28 ($B_T=15.87$, $D_{25}=0.6$, Sbc) and 2MASXi J1014531-205752 (=PGC 834527), with $B_T=16.19$ and $D_{25}=0.8$.

L447O: 2MASXJ11174025+3803095 = UGC 6307: our profile has a 58 km s $^{-1}$ lower central velocity than the Green Bank 91m profile of Schneider et al. (1992), although the W_{50} line widths are the same (206 km s $^{-1}$). The Nançay integrated line flux is 1.4 times higher. No candidates for confusion within the telescope beams are visible on the DSS.

L455O: 2MASXIJ1128100+165531 = NGC 3691: our profile ($V_{HI}=987$ km s $^{-1}$) has an on average 100 km s $^{-1}$ lower central velocity than the 4 published H_I spectra, three of which were measured at Arecibo and one with the Green Bank 91m telescope (see Table 2). The line widths and integrated line fluxes are in agreement, however. The optical systemic velocity of 997 ± 38 km s $^{-1}$ (Blackman 1980) is in good agreement with our centre velocity. The Nançay profile has a peculiar shape and may in principle have been affected by RFI. No candidates for confusion within the telescope beams are visible on the DSS.

L459O: 2MASXJ11375027+4752539 = NGC 3769A: the H_I profile of the target galaxy is confused with that of NGC 3769, the much larger spiral with which it forms a close pair. Our H_I profile ($V_{HI}=734$ km s $^{-1}$, $W_{50}=230$ km s $^{-1}$, $I_{HI}=35.0$ Jy km s $^{-1}$) is in agreement with the mean of the literature values of $V_{HI}=732$ km s $^{-1}$, $W_{50}=232$ km s $^{-1}$ and $I_{HI}=50.6$ Jy km s $^{-1}$ (Magri 1994; Rhee & van Albada 1996; Verheijen & Sancisi 2001). The latter refers to a mapping of the pair with the WSRT.

L481O: 2MASXJ11562491-1210003 = MCG -02-31-002: our H_I spectrum shows two peaks, at $V_{HI}=5429$ and 11,891 km s $^{-1}$, respectively. The latter detection appears to have its high-velocity edge clipped by negative RFI. The target galaxy ($B_T=15.4$, $D_{25}=1.2$) does not have a known optical redshift and there is no other galaxy in the search area likely to cause confusion in the Nançay beam.

L497O: 2MASXIJ1212205+291240 = NGC 4173: Our H_I spectrum shows two detections, at $V_{HI}=1054$ and 3795 km s $^{-1}$, respectively. The former is due to the target galaxy, at $V_{opt}=1117\pm32$ km s $^{-1}$, while the latter is due to three other galaxies in the beam (NGC 4169, 4174 and 4175), which have optical redshifts in the range of 3780-4000 km s $^{-1}$. The redshift of our profile of NGC 4173 ($V_{HI}=1054$ km s $^{-1}$, $W_{50}=163$ km s $^{-1}$, $I_{HI}=27.6$

Jy km s $^{-1}$) is 53 km s $^{-1}$ higher than the mean LEDA values ($V_{HI}=1107$ km s $^{-1}$, $W_{50}=116$ km s $^{-1}$, $I_{HI}=13.4$ Jy km s $^{-1}$) and its integrated line flux is twice as high.

L502P: 2MASXIJ1216418-251505 = PGC 781011: two peaks are seen in our H_I spectrum, at 451 and 5708 km s $^{-1}$, respectively. On the DSS no obvious candidate could be found that might correspond to the former H_I signal ($V_{HI}=451$ km s $^{-1}$, $W_{50}=65$ km s $^{-1}$, $I_{HI}=1.1$ Jy km s $^{-1}$). We assume that the latter peak ($V_{HI}=5708$ km s $^{-1}$, $W_{50}=62$ km s $^{-1}$, $I_{HI}=1.6$ Jy km s $^{-1}$) corresponds to the target galaxy ($B_T=16.1$, $D_{25}=0.5$).

L548O: 2MASXJ12503459-0931108 = MCG -01-33-022: our H_I profile of the target galaxy ($V_{HI}=4689$ km s $^{-1}$, $W_{50}=274$ km s $^{-1}$, $I_{HI}=4.0$ Jy km s $^{-1}$), with an optical redshift of 4666 ± 80 km s $^{-1}$, is very probably confused with that of a nearby pair of galaxies, NGC 4716/7. NGC 4716 is an S0 with $V_{opt}=4573\pm119$ km s $^{-1}$ and NGC 4717 is a spiral with $V_{opt}=4515\pm96$ kms; none of them has previously been reported as detected in H_I.

L569O: 2MASXJ13165624-1635347 = MCG -03-34-040: the target galaxy is seen superposed on the outermost regions of a much larger Sbc spiral, NGC 5054, which will dominate the H_I profile. Our H_I line parameters ($V_{HI}=1682$ km s $^{-1}$, $W_{50}=321$ km s $^{-1}$, $I_{HI}=14.8$ Jy km s $^{-1}$) are quite different the mean published values of NGC 5054 $V_{HI}=1741$ km s $^{-1}$, $W_{50}=315$ km s $^{-1}$, $I_{HI}=26.8$ Jy km s $^{-1}$ (Bottinelli et al. 1982; Fisher & Tully 1981; Richter & Huchtmeier 1987; Shostak 1978).

L582O: 2MASXJ13324730+4151564 = ESO 579-G5: the target galaxy is seen superposed on the outer regions of a much larger Sc spiral, NGC 5214, which will dominate the H_I profile. Our H_I line parameters ($V_{HI}=8174$ km s $^{-1}$, $W_{50}=303$ km s $^{-1}$, $I_{HI}=7.6$ Jy km s $^{-1}$) are similar to the published values of NGC 5124 $V_{HI}=8180$ km s $^{-1}$, $W_{50}=306$ km s $^{-1}$, $I_{HI}=4.9$ Jy km s $^{-1}$ (Haynes & Giovanelli 1991). In the same beam as the target galaxy ($B_T=15.8$, $D_{25}=1.0$, Sbc), lies the somewhat fainter Sab ESO 579-G6 ($B_T=16.2$, $D_{25}=0.8$). Since neither has a known optical redshift, it cannot be determined if their proximity could cause confusion in our H_I spectrum.

(F40O) = MCG -2-36-13: the radial velocity of the detected line profile, 4882 km s $^{-1}$, is completely different from the optical value of 12,500 km s $^{-1}$ (da Costa et al. 1998), which lies far outside our velocity search range. No candidate was found for confusion within the beam. The observed line signal may be spurious and due imperfectly filtered to RFI.

L643O: 2MASXIJ1447561-141658 = MCG-02-38-015: the target object corresponds to an outer spiral arm of the spiral MCG-02-38-015. Our H_I profile parameters ($V_{HI}=1927$ km s $^{-1}$, $W_{50}=221$ km s $^{-1}$, $I_{HI}=22.3$ Jy km s $^{-1}$) show a 66 km s $^{-1}$ lower mean velocity than the average of the literature values, $V_{HI}=2046$ km s $^{-1}$, $W_{50}=199$ km s $^{-1}$ and $I_{HI}=23.4$ Jy km s $^{-1}$ (Theureau et al. 1998; Thonnard et al. 1978).

L647O: 2MASXJ14563333-2430079 = ESO 513-G009: our H_I spectrum shows two peaks, at $V_{HI}=6894$ and 8600 km s $^{-1}$, respectively. The optical redshift of the target

galaxy, $6815 \pm 44 \text{ km s}^{-1}$, corresponds to the lower velocity peak. No galaxy could be identified that may have caused the other peak.

L651O: 2MASXJ15064639+1251009 = CGCG 077-007: the H_I profile of the target galaxy, ($V_{opt}=6582 \pm 105 \text{ km s}^{-1}$, $B_T=16.1$, $D_{25}=0'7$) will be confused with that of NGC 5851 ($V_{opt}=6515 \pm 64 \text{ km s}^{-1}$, $B_T=14.2$, $D_{25}=1'0$), at 1.8 E of the 2MASS object, i.e. around the Nançay HPBW. Our H_I profile shows $V_{HI}=6576 \text{ km s}^{-1}$, $W_{50}=43 \text{ km s}^{-1}$ and $I_{HI}=5.5 \text{ Jy km s}^{-1}$, while the Nançay profile of NGC 5851 (Bottinelli et al. 1999) shows $V_{HI}=6508 \text{ km s}^{-1}$, $W_{50}=281 \text{ km s}^{-1}$ and $I_{HI}=2.3 \text{ Jy km s}^{-1}$.

L654P: 2MASXJ15205260-2859139 = PGC 160462: our H_I spectrum shows two peaks, at $V_{HI}=3934$ and 6022 km s^{-1} , respectively. The target galaxy has no known optical redshift and no other galaxy was found in the search area. It is not clear with which of the two H_I lines it is associated.

L705O: 2MASXIJ1719223+490202 = VV 010b: our H_I spectrum ($V_{HI}=7478 \text{ km s}^{-1}$, $W_{50}=97 \text{ km s}^{-1}$, $I_{HI}=2.6 \text{ Jy km s}^{-1}$) will be confused by that of the interacting pair Arp 102 (PGC 60067/70); the centre of PGC 60070 lies only $0'5$ from that of the much smaller Sd target galaxy, PGC 60073 ($B_T=16.2$, $D_{25}=0'7$). PGC 60070 is an Sd with $V_{opt}=7177 \pm 35 \text{ km s}^{-1}$, $B_T=15.5$ and $D_{25}=1'1$, and PGC 60067 an elliptical with $V_{opt}=7304 \pm 99 \text{ km s}^{-1}$, $B_T=15.5$ and $D_{25}=0'95$.

L712O: 2MASXJ18030213+2922257 = CGCG 171-049: the H_I spectrum ($V_{HI}=7048 \text{ km s}^{-1}$, $W_{50}=473 \text{ km s}^{-1}$, $I_{HI}=3.3 \text{ Jy km s}^{-1}$) of the target galaxy ($V_{opt}=7048 \pm 46 \text{ km s}^{-1}$, $B_T=15.7$, $D_{25}=0'8$) may be confused by another galaxy in the telescope beam, CGCG 171-048 ($V_{opt}=6983 \pm 44 \text{ km s}^{-1}$, $B_T=15.4$, $D_{25}=0'75$).

L745O: 2MASXJ20170275-1206516 = MCG -02-51-007: the H_I spectrum ($V_{HI}=5656 \text{ km s}^{-1}$, $W_{50}=355 \text{ km s}^{-1}$, $I_{HI}=5.8 \text{ Jy km s}^{-1}$) of the target galaxy ($B_T=15.6$, $\log(D_{25})=0'8$, Sb), without known optical redshift, may be confused by another galaxy in the telescope beam, MCG -02-51-008 ($V_{opt}=5578 \pm 60 \text{ km s}^{-1}$, $B_T=14.3$, $D_{25}=0'6$, Sc).

L752O: = FGC 2286: our profile has a 43 km s^{-1} lower central velocity than the Nançay profile of Matthews & van Driel (2000), although the line widths and integrated line fluxes are comparable (see Table 2).

L755O: 2MASXJ20481195-0352186 = MCG -01-53-009: the H_I spectrum ($V_{HI}=6042 \text{ km s}^{-1}$, $W_{50}=128 \text{ km s}^{-1}$, $I_{HI}=1.2 \text{ Jy km s}^{-1}$) of the target galaxy ($V_{opt}=5945 \pm 60 \text{ km s}^{-1}$, $B=13$, $D_{25}=1'1$), may in principle be confused by an object of similar size but lower surface brightness at only $0'9$ separation, MCG -01-53-010 ($B=15$, $D_{25}=1'0$), without known redshift.

L758O: 2MASXJ20550682-3105304 = ESO 463-IG34: the target galaxy is a close interacting pair of galaxies.

L766O: 2MASXJ21455799-3448541 = ESO 403-G23: our H_I spectrum shows two peaks, at $V_{HI}=5140$ and $12,924 \text{ km s}^{-1}$, respectively. No other galaxy was found in the search area besides the target galaxy ($B_T=15.4$,

$D_{25}=1'2$, Sc), without known optical redshift. Seen the galaxy's optical parameters, it is most likely with the H_I emission at 5140 km s^{-1} .

L777P: 2MASXIJ2216009-095612 = PGC 984498: the target galaxy ($B_T=16.5$, $D_{25}=0'5$), shows two nuclei on the DSS and 2MASS images, as well as a tidal tail on the DSS. There is another galaxy of similar magnitude in the beam, 2MASXi J2216005-095324 ($B_T=16.5$, $D_{25}=0'9$), also without optical redshift.

L783O: 2MASXJ22230550-2857173 = NGC 7259: the H_I spectrum ($V_{HI}=1657 \text{ km s}^{-1}$, $W_{50}=152 \text{ km s}^{-1}$, $I_{HI}=11.6 \text{ Jy km s}^{-1}$) of the target galaxy ($V_{opt}=1718 \pm 42 \text{ km s}^{-1}$, $B_T=13.6$, $D_{25}=1'2$), will be confused by an edge-on galaxy at $2'8$ distance, ESO 467-G51 ($V_{opt}=1775 \pm 32 \text{ km s}^{-1}$, $B_T=14.6$, $D_{25}=2'8$), of which Theureau et al. (1998) obtained an H_I profile at Nançay with $V_{HI}=1808 \text{ km s}^{-1}$, $W_{50}=146 \text{ km s}^{-1}$, $I_{HI}=18.6 \text{ Jy km s}^{-1}$.

L794O: 2MASXIJ2244347-225930 = ESO 534-G21: the H_I profile of the target galaxy will not be confused by its close apparent companion, eso-lv 5340211 at only $0'3$ distance, as their optical redshifts are 3159 and 18,116 km s^{-1} , respectively.

5. Discussion

A comparison of the global parameters of the H_I profiles measured for our survey at Nançay with those obtained from the literature is given in Table 2. Indicated with a '*' after the source name in column 1 are the cases in which profile(s) are likely to be confused with those of other galaxies in the telescope beam(s), see Section 4.5 for further details. We also compared the line parameters of the 18 calibrator galaxies observed throughout the survey.

Plotted in Figures 4, 5 and 6 are, respectively, the differences between central line velocities from our survey and from the literature, survey and literature W_{50} line widths and I_{HI} integrated line fluxes for the 2MASS survey galaxies with non-confused spectra as well as for the calibration galaxies.

The agreement between the central H_I velocities is generally good (Fig. 4). The 4 survey galaxies for which the literature values are (on average) more than 40 km s^{-1} different from our values are L447O (UGC 6307), L455O (NGC 3691), L643O (MCG 2-38-15) and L752O (FGC 2286), see Section 4.5 for comments. In general no clear cause can be identified for these discrepancies, although RFI in our data may be involved in some cases.

The agreement between the W_{50} line widths is generally good (Fig. 5), with two exceptions. These two discrepancies, of about -80 km s^{-1} , for L497O (NGC 4173) and calibration galaxy NGC 3321 (PGC 31653) are due to one anomalously narrow published line width per galaxy, while all other literature values are in agreement with ours.

A comparison between the integrated line fluxes I_{HI} (Fig. 6) shows a larger scatter for the survey objects than the two other plots, which appears reasonable, however, seen the dispersion found in other such plots (e.g., van Driel et al. 2000). The three cases in which a literature

value exceed our measurement by more than a factor 2 are L6O (NGC 45), which is considerably larger than the Nançay beam, L445O (IC 2627), which may well have been resolved by the Nançay beam and L487O (UGC 7000), due to the anomalously high Arecibo value of Impey et al. (1996).

The fluxes of the calibrator galaxies are in good agreement with the literature values. Comparing to measurements made with other telescopes, which are available for 7 galaxies, we find that our I_{HI} values are on average 0.95 ± 0.25 times these values. Comparing to the Nançay measurements of 18 galaxies by Theureau et al. (1998), which were made with the previous receiver system (see Section 3), we find a scaling factor of 1.10 ± 0.22 . The standard deviations in these scaling factors are only slightly larger than the $\sim \pm 15\%$ accuracy of the internal calibration of the Nançay data (e.g., Matthews et al. 2001).

There are 4 survey galaxies (L180O = FGC 410, L467O = UGC 6679, L630O = ESO 447-5 and L673O = MCG 3-41-136) that did not meet our criteria for clear or marginal detections, which were reported as detected in the literature (see Table 2). All four were observed by us in the low-velocity search mode only, i.e. in the -500 to 10,500 km s $^{-1}$ range, which means that the systemic velocity of L630O (10,600 km s $^{-1}$) lies just outside our search range. The other three were detected in the Nançay survey of Matthews & van Driel (2000), which has a significantly lower noise level than the present survey.

6. Conclusions

Of the 334 galaxies observed in total, 171 (51%) were clearly detected, 76 of which did not have a previously known radial velocity. The detection statistics as function of type (previously catalogued (PGC/other catalogues) or not) and size/selection algorithm (Large/Faint) are listed in table 1. For the Large objects ($r_{K_{20}} \geq 20''$) and the Faint objects (selected with the LCSB source processor), the overall detection rates are quite similar: 51% and 56%, respectively.

Acknowledgements. This publication makes use of data products from the Two Micron All Sky Survey, which is a joint project of the University of Massachusetts and the Infrared Processing and Analysis Center, funded by the National Aeronautics and Space Administration and the National Science Foundation. The Nançay Radio Observatory, which is the Unité Scientifique de Nançay of the Observatoire de Paris, is associated with the French Centre National de Recherche Scientifique (CNRS) as USR B704, and acknowledges the financial support of the Région Centre as well as of the European Union. This research also has made use of the Lyon-Meudon Extragalactic Database (LEDA), recently incorporated in HyperLeda, the NASA/IPAC Extragalactic Database (NED) which is operated by the Jet Propulsion Laboratory, California Institute of Technology, under contract with the National Aeronautics and Space Administration and the Aladin database, operated at CDS, Strasbourg, France. We acknowledge financial support from CNRS/NSF collaboration grant No. 10637.

References

- Allen, C. W. 1973, *Astrophysical Quantities* (Athlone Press, London)
- Bajaja, E. 1979, *Pub. Univ. Chile*, 3, 64
- Balkowski, C. 1979, *A&A*, 78, 190
- Bergvall, N., Rönnback, J., Masegosa, J., & Östlin, G. 1999, *A&A*, 341, 697
- Bicay, M. D., & Giovanelli, R. 1986, *AJ*, 91, 732
- Blackman, C. P. 1980, *MNRAS*, 191, 123
- Boissier, N., Prantzos, N., Monnier Ragaigne, D., van Driel, W., Balkowski, C., & O'Neil, K. 2003, *MNRAS*, in press (astro-ph/0304313)
- Boselli, A., Gavazzi, G., Franzetti, P., Pierini, D., & Scoggio, M. 2000, *A&A*, 142, 73
- Bothun, G. D., Aaronson, M., Schommer, R. A., et al. 1985, *ApJS*, 57, 423
- Bothun, G. D., Impey, C. D., Malin, D. F., & Mould, J. R. 1987, *AJ*, 94, 23
- Bottinelli, L., Gouguenheim, L., & Paturel, G. 1980, *A&A*, 88, 32
- Bottinelli, L., Gouguenheim, L., & Paturel, G. 1982, *A&A*, 113, 61
- Bottinelli, L., Gouguenheim, L., Theureau, G., Coudreau, N., & Paturel, G. 1999, *A&AS*, 135, 429
- Chamaraux P., Masnoux J. L., Kazes I., et al. 1999, *MNRAS*, 307, 236
- Chung, A., van Gorkom, J. H., O'Neil, K., & Bothun, G. D. 2002, *AJ*, 123, 2387
- da Costa, L. N., Willmer, C. N. A., Pellegrini, P. S., et al. 1998, *AJ*, 116, 1
- Davies, R. D. 1980, Private Communication
- Davis, L. E., & Sequist, E. R. 1983, *ApJS*, 53, 269
- Dean, J. F., & Davies, R. D. 1975, *MNRAS*, 170, 503
- de Vaucouleurs, G., de Vaucouleurs, A., Corwin, H. G., et al. 1991, *The Third Reference Catalogue of Bright Galaxies* (Springer-Verlag, New York) (RC3)
- Fisher, J. R., & Tully, R. B. 1975, *ApJS*, 44, 151
- Fisher, J. R., & Tully, R. B. 1981, *ApJS*, 47, 139
- Freudling, W. 1995, *A&AS*, 112, 429
- Fridman, P. A., & Baan, W. A. 2001, *A&A*, 378, 327
- Fouqué, P., Bottinelli, L., Durand, N., Gouguenheim, L., & Paturel, G. 1990, *A&AS*, 86, 473
- Garcia-Bareto, J. A., Downes, D., & Huchtmeier, W. K. 1994, *A&A*, 288, 705
- Giovanardi, C., & Salpeter, E. E. 1985, *ApJS*, 58, 623
- Grogan, N. A., & Geller, M. J. 2000, *AJ*, 119, 32
- Haynes, M. P., Giovanelli, R., Starosta, B. M., & Magri, C. 1988, *AJ*, 95, 607
- Haynes, M. P., & Roberts, M. S. 1979, *ApJ*, 227, 767
- Haynes, M. P., & Giovanelli, R. 1991, *A&AS*, 77, 331
- Haynes, M. P., Giovanelli, R., Herter, T., et al. 1997, *AJ*, 113, 1197
- Haynes, M. P., Giovanelli, R., Chamaraux, P., et al. 1999, *AJ*, 117, 2039
- ITU-R Radio Regulations 2001, International Telecommunication Union (Geneva, Switzerland)
- Helou, G., Salpeter, E. E., & Terzian, Y. 1982, *AJ*, 87, 1443
- Huchra, J. H., Latham, D. W., da Costa, L. N., et al. 1993, *AJ*, 105, 1637
- Huchtmeier, W. K., Seiradakis, J. H., & Materne, J. 1981, *A&A*, 102, 134
- Huchtmeier, W. K. 1982, *A&A*, 110, 121
- Huchtmeier, W. K., & Seiradakis, J. H. 1985, *A&A*, 143, 216

- Huchtmeier, W. K., Karachentsev, I. D., Karachentseva, V. E., & Ehle, M. 2000, A&AS, 141, 469
- Hurt, R. L., Jarrett, T. H., Kirkpatrick, J. D., et al. 2000, AJ, 120, 1876
- Impey, C. D., Sprayberry, D., Irwin, J. A., & Bothun, G. D. 1996, ApJS, 105, 209
- Jarrett, T. H., Chester, T., Cutri, R., et al. 2000a, AJ, 119, 2498
- Jarrett, T. H., Chester, T., Cutri, R., et al. 2000b, AJ, 120, 298
- Kraan-Korteweg, R. C., van Driel, W., Briggs, F., Binggeli, B., & Mostefaoui, T. I. 1999, A&AS, 135, 255
- Lewis, B. M. 1972, Aust. J. Phys., 25, 315
- Lewis, B. M., 1983, AJ, 88, 962
- Lewis, B. M., Helou G., & Salpeter, E. E. 1985, ApJS, 59, 161
- Magri, C. 1994, AJ, 108, 896
- Mathewson, D. S., & Ford, V. L. 1996, ApJS, 107, 97
- Matthews, L. D., & van Driel, W. 2000, A&A, 143, 421
- Matthews, L. D., van Driel, W., & Monnier-Ragaigne, D. 2001, A&A 365, 1
- McGaugh, S. S., & de Blok, W. J. G. 1997, ApJ, 481, 689
- McGaugh, S. S., Rubin, V. C., & de Blok, W. J. G. 2001, AJ 122, 2381
- Monnier Ragaigne, D., van Driel, W., Schneider, S. E., Jarrett, T. H., & Balkowski, C. 2003a, A&A, in press (paper I) (astro-ph/0304380)
- Monnier Ragaigne, D., van Driel, W., Schneider, S. E., O'Neil, K., Balkowski, C., & Jarrett, T. 2003b, A&A, in press (paper II) (astro-ph/0304553)
- Monnier Ragaigne, D., Papaderos, P., van Driel, W., Testor, G., Plana, H., Balkowski, C., Schneider, S. E., & Jarrett, T. H. 2003d, A&A, in preparation (paper IV)
- Mould J. R., Akeson R. L., Bothun G. D., et al. 1993, ApJ, 409, 14
- O'Neil, K., Bothun, G. D., & Cornell, M. E. 1997a, AJ, 113, 1212
- O'Neil, K., Bothun, G. D., Schombert, J., Cornell, M. E., & Impey, C. D 1997b, AJ, 114, 2448
- O'Neil, K., Bothun, G. D., & Schombert, J. 2000, AJ 119, 136 113, 905
- Paturel, G., Bottinelli, L., Di Nella, H., et al. 1997, A&AS, 124, 109
- Paturel, G., Theureau, G., Bottinelli, L., et al. 2002, A&A, in preparation
- Peterson, S. D., & Shostak, G. S. 1974, AJ, 79, 767
- Reif K., Mebold U., Goss W. M., van Woerden H., & Siegman B. 1982, A&AS, 50, 451
- Rhee, G., & van Albada, T. S. 1996, A&AS, 115, 407
- Richter, O.-G., & Huchtmeier W. K. 1987, A&AS, 68, 427
- Rogstad, D. H., Rougoor, G. W., & Whiteoak, J. B. 1967, ApJ, 150, 9
- Rosenberg, J. L., & Schneider, S. E. 2000, ApJS, 130, 177
- Schneider, S. E., Helou G., Salpeter, E. E., & Terzian, Y. 1986, AJ, 92, 742
- Schneider, S. E., Thuan, T. X., Mangum, J. G., & Miller, J. 1992, ApJS, 81, 5
- Schneider, S., Huchra, J., Jarrett, T., & Chester, T. 1997, 2MASS Extragalactic Studies: Early Results from the Prototype Camera, in The Impact of Large-Scale Near-IR Sky Surveys, ed. F. Garzon et al. (Kluwer, Dordrecht), 231
- Schommer R.A., Sullivan III, W. T., & Bothun G. D. 1981, AJ, 86, 943
- Shostak G.S. 1978, A&A, 68, 321
- Spitzak, J. G., & Schneider, S. E. 1998, ApJS, 119, 159
- Staveley-Smith, L., & Davies, R. D. 1987, MNRAS, 224, 953
- Sulentic, J. W., & Arp, H. 1983, AJ, 88, 489
- Theureau, G., Bottinelli, L., Coudreau-Durand, N., et al. 1998, A&AS, 130, 333
- Thonnard, N., Rubin, V. C., Ford Jr., W. K., & Roberts, M. S. 1978, AJ, 83, 1564
- Tifft W. G., & Cocke W. J. 1988, ApJS, 67, 1
- van den Hoek, L. B., de Blok, W. J. G., van der Hulst, J. M., & de Jong, T. 2000, A&A, 357, 397
- van Driel, W., Pezzani, J., & Gérard, E. 1997, Renovating the Nançay radio telescope: the FORT project, in High-sensitivity Radio Astronomy, ed. N. Jackson & R.J. Davies (Cambridge Univ. Press, Cambridge), 229
- van Driel, W., Arnaboldi, M., Combes, F., & Sparke, L. S. 2000, A&AS, 141, 385
- van Driel, W., Marcum, P., Gallagher III, J.S., et al. 2001, A&A, 378, 370
- van der Hulst, J.M., Skillman, E. D., Smith, T. R., et al. 1993, AJ, 106, 548
- van Zee, L., Haynes, M. P., & Salzer, J. J. 1997, Star Formation Activity in High M/L Galaxies, in Dwarf Galaxies: Probes for galaxy formation and Evolution, Joint Discussion, Kyoto, Japan, 14
- Verheijen, M. A. W., & Sancisi, R. 2001, A&A, 370, 765

Table 1. H_I detection statistics

	Previously Catalogued (Other)		Previously Catalogued (PGC)		Previously Uncatalogued (New)		All
	Large	Faint	Large	Faint	Large	Faint	
Total observed	229	14	41	0	39	11	334
Detected	140	61%	10	71%	12	29%	0 0%
Marginal	23	10%	0	0%	0	0%	0 0%
Undetected	66	29%	4	29%	29	71%	0 0%
					34	87%	7 64%
							139 42%

Note: Large: galaxies with $r_{K20} \geq 20''$, Faint: galaxies selected using the LCSB source processor.

Table 2. Comparison with published H I data

No.	PGC	Ident.	V_{HI} km/s	W_{50} km/s	I_{HI} Jy km/s	Tel.	Ref.
Clearly detected galaxies							
L6O	0930	NGC 45	467	156	66.2	N	this paper
			474	—	G43		Haynes & Roberts (1979)
			461	—	—	IAR	Bajaja (1979)
			468	—	—	P	Reif et al. (1982)
			470	—	211	E	Huchtmeier et al. (1981)
			470	172	217	O	Rogstad et al. (1967)
			467	165	—	J	Dean & Davies (1975)
			471	—	227	G43	Fisher & Tully (1975)
			471	174	238	G43	Fisher & Tully (1981)
			468	167	242	E	Huchtmeier & Seiradakis (1985)
			459	—	384	P	Lewis (1972)
L53O	4650	UGC 825	5334	289	2.5	N	this paper
			5338	292	2.7	N	Matthews & van Driel (2000)
L57O*	4734	UGC 847	5240	266	2.4	N	this paper
			5238	265	2.7	G	Haynes & Giovanelli (1991)
L99O	8078	UGC 1601	5567	225	5.7	N	this paper
			5591	260	6.9	E	Haynes et al. (1999)
L117O*	9431	NGC 948	4755	165	2.7	N	this paper
			4487	181	6.0	G43	Haynes et al. (1999)
L125O*	9831	NGC 980	5733	582	4.0	N	this paper
			5757	—	8.1	G	Magri (1994)
			5737	702	8.2	G	Haynes et al. (1988)
L182O	12664	MCG -2-9-36	2801	215	15.2	N	this paper
			2808	222	18.4	G	Fisher & Tully (1981)
			2806	—	19.4	G	Tifft & Cocco (1988)
L336O	23319	UGC 4329	4096	218	6.8	N	this paper
			4092	—	7.8	A	Schombert et al. (1981)
			4098	224	—	A	Lewis (1983)
			4090	232	7.5	A	Bothun et al. (1985)
			4098	243	7.0	A	Lewis et al. (1985)
			4095	221	8.2	A	Bicay & Giovanelli (1986)
			4100	—	8.4	G	Tifft & Cocco (1988)
			4106	212	6.0	A	Rosenberg & Schneider (2000)
L345O*	23977	ESO 495-17	1476	201	3.2	N	this paper
			1467	179	3.7	N	Chamaraux et al. (1999)
L352O	24489	ESO 563-16	1732	184	16.4	N	this paper
			1732	180	16.6	N	Fouqué et al. (1990)
L360O*	25281	NGC 2719	3077	211	9.3	N	this paper
			3157	203	15.7	A	Bicay & Giovanelli (1986)
			3167	—	16.7	G	Davis & Seaquist (1983)
L364O	25472	UGC 4753	1828	159	2.1	N	this paper
			1851	172	3.9	N	Matthews & van Driel (2000)
L371O*	26238	NGC 2799	1673	156	9.1	N	this paper
			1755	343	11.1	N	Bottinelli et al. (1982)
			1750	304	10.9	N	van Driel et al. (2001)
L430O	32204	UGC 5879	5612	278	5.5	N	this paper
			5612	283	5.4	N	Matthews & van Driel (2000)
L445O	33860	IC 2627	2087	50	10.8	N	this paper
			2075	34	18.4		Davies (1980)
			2090	40	24.2	E	Fisher & Tully (1981)
			2082	39	24.8	E	Richter & Huchtmeier (1987)
			2075	—	21.9	P	Reif et al. (1982)
L447O	34497	UGC 6307	1906	207	7.5	N	this paper
			1964	206	5.2	G	Schneider et al. (1992)
L455O	35292	NGC 3691	987	125	2.9	N	this paper
			1067	125	2.6	A	Helou et al. (1982)
			1071	145	4.0	A	Giovanardi & Salpeter (1985)
			1080	128	3.1	A	Lewis et al. (1985)
			1113	—	5.0	G	Tifft & Cocco (1988)
L487O	37914	UGC 7000	1492	80	6.1	N	this paper
			1483	67	5.7	A	Sulentic & Arp (1983)
			1487	75	5.5	A	Schneider et al. (1986)
			1498	79	5.9	A	Schneider et al. (1986)
			1487	—	7.52	G	Richter & Huchtmeier (1987)
			1475	—	21.1	A	Impey et al. (1996)

Note: a * following a name in column (1) indicates a confused spectrum, see Section 4.5.

Table 2. Comparison with published H I data – *continued*

No.	PGC	Ident.	V_{HI} km/s	W_{50} km/s	I_{HI} Jy km/s	Tel.	Ref.
Clearly detected galaxies – continued							
L497O	38897	NGC 4173	1120	160	27.6	N	this paper
			1127	170	42.1	G	Fisher & Tully (1981)
			1085	80	19.8	A	Bothun et al. (1985)
			1127	—	—	E	Garcia-Bareto et al. (1994)
			1096	164	34.2	N	Kraan-Korteweg et al. (1999)
L512O	40092	IC 784	4872	387	9.2	N	this paper
			4865	—	11.0	G	Richter & Huchtmeier (1987)
			4876	—	6.2	N	Paturel et al. (2002)
L572O	46664	NGC 5105	2902	214	9.9	N	this paper
			2904	—	14.95	G	Richter & Huchtmeier (1987)
			2903	215	14.52	G	Haynes et al. (1999)
F38O	48621	UGC 8688	1359	60	5.0	N	this paper
			1355	63	5.4	E	Huchtmeier et al. (2000)
L634O	52012	CGCG 133-87	4782	230	4.7	N	this paper
			4781	259	5.9	A	Mould et al. (1993)
			4783	—	2.8	A	Freudling (1995)
L639O	52612	ESO 580-14	6080	96	3.3	N	this paper
			6080	82	3.1	N	Fouqué et al. (1990)
L643O	52853	MCG-2-38-15	1979	217	22.3	N	this paper
			2045	200	23.4	G	Thonnard et al. (1978)
			2046	—	—	N	Theureau et al. (1998)
L735O	63425	ESO 594-8	6136	325	4.4	N	this paper
			6140	345	6.0	G	Haynes et al. (1999)
L746O	64448	ESO 462-7	6130	323	6.9	N	this paper
			6132	331	8.7	N	Haynes et al. (1999)
L752O	91678	FGC 2286	3783	245	3.7	N	this paper
			3825	256	3.2	N	Matthews & van Driel (2000)
L781O	68645	UGC 11999	3287	162	2.0	N	this paper
			3298	174	2.5	N	Matthews & van Driel (2000)
L788O	68996	IC 1447	2953	315	3.7	N	this paper
			2967	291	4.8	N	Theureau et al. (1998)
Marginally detected galaxies							
L739O	63776	ESO 526-11	5855	292	2.5	N	this paper
			5844	300	1.9	N	Paturel et al. (2002)
			5855	294	2.5	N	Haynes et al. (1999)
Undetected galaxies							
L180O	12439	FGC 410	—	—	<4.0	N	this paper
			2756	236	3.0	N	Matthews & van Driel (2000)
L467O	36381	UGC 6679	—	—	<2.5	N	this paper
			5172	326	2.8	N	Matthews & van Driel (2000)
L630O	51628	ESO 447-5	—	—	<3.6	N	this paper
			7128	273	3.2	N	Matthews & van Driel (2000)
L673O	57278	MCG 3-41-136	—	—	<2.3	N	this paper
			10596	452	1.2	A	Bothun et al. (1985)
			10627	452	1.6	A	Haynes et al. (1997)

Note: a * following a name in column (1) indicates a confused spectrum, see Section 4.5.

Telescope codes:

A	Arecibo 305-m
E	Effelsberg 100-m
G	Green Bank 90-m
G43	Green Bank 43-m
IAR	I.A.R. 30-m
J	Jodrell Bank 76-m
N	Nançay 94-m equiv.
O	Owens Valley
P	Parkes 64-m

Table 3a.1. Detected objects
– identifications and coordinates

Number	2MASS hhmmss.s+ddmmss (J2000.0)	PGC	others
L6O	0014039-231054	930	MCG -04-01-021
L8O	0019256-040456	1261	MCG -01-01-077
L9O	0020006-062008	1288	MCG -01-02-001
L17O	0030459-292034	1879	ESO 410-G16
(F2O)	0041167-051707	2470	MCG -01-02-045
L29O	0041576-325810	2510	ESO 351-G2
L39O	0105188-052520	3861	MCG -01-03-089
L45O	0110374-031324	4192	MCG -01-04-006
L52O	0115539-322838	4566	ESO 352-G30
L53O	0117369+490042	4650	UGC 0825
L57O	0119042-000819	4734	UGC 0847
L59O	0122228-363630	4991	ESO 352-G58
L61O	0128568-163059	5532	MCG -03-04-075
L62O	0129399-221927	5571	ESO 476-G14
L70O	0143029-341114	6319	IC 1722
L78O	0154524-133915	7109	MCG -02-05-074
L84O	0158502-304004	7481	ESO 414-G19
L86O	0159074-030859	7507	MCG -01-06-013
L87O	0159117-274838	7514	IC 1763
L91O	0201303-071731	7682	KUG 0159-075
L93O	0201511-102803	7714	MCG -02-06-017
L99O	0207082+425756	8078	UGC 1601
L117O	0228454-103047	9431	NGC 948
L120N	0232053-112516		
(L125O)	0235204+405522	9831	NGC 980
L137O	0242460-212802	10271	ESO 546-G11
L138O	0243380-315641	10326	ESO 416-G12
L144P	0251205-304655	10831	
L157O	0303243-153725	11503	NGC 1189
L169O	0313315-151526	12008	MCG -03-09-010
L170O	0314054-214627	12034	NGC 1258
L181O	0322416-041118	12650	NGC 1314
L182O	0322558-111207	12664	MCG -02-09-036
L184O	0323483+403348	12702	UGC 2708
(L191O)	0330358-175630	13029	ESO 548-G28
(L192O)	0332576-210521	13150	ESO 548-G34
L198O	0336173-253616	13304	ESO 482-G11
L203O	0340415-223904	13532	ESO 482-G31
L204O	0340571-214249	13543	NGC 1414
L211O	0346556-114820	961488	FGC 0452
L214O	0350397-251646	13952	ESO 482-G47
L215O	0350433-025141	13951	MCG -01-10-041
L219O	0353180-102645	14037	MCG -02-10-018
L220O	0355047-061316	14100	MCG -01-10-047
L223O	0400416-304951	14271	ESO 419-G13
L225O	0409253-040927	14571	MCG -01-11-003
L226O	0410502-295535	14607	ESO 420-G8
L237O	0429408-272430	15292	NGC 1592
L243O	0437498-122635	15688	MCG -02-12-048
L244O	0440148-241907	15780	ESO 485-G6
L252O	0446072-020438	15958	NGC 1657
L255O	0451183-055738	16163	MCG -01-13-021
L256O	0455154-120927	16329	MCG -02-13-023
L260O	0500455-295129	16543	ESO 422-G20
L261O	0501015-085726	16553	MCG -02-13-036
(L270O)	0510143-292359	16854	ESO 422-G40
L272O	0515387-224232	16990	ESO 486-G40
F16O	0527059-204041	17302	ESO 553-G46
(F17O)	0527012-213326	17301	ESO 553-G45
L289O	0558023-125546	148136	NPM1G -12.0210
L296P	0609212-140823	928447	
L297O	0613188+530644	18651	UGC 3421
(F18N)	0623041-350604		
L301O	0623256-160943	18930	MCG -03-17-004
L302O	0624392-223549	18983	ESO 489-G50
L303O	0626230-314736	19047	ESO 426-G9
L304N	0627010-123153		
L308O	0643196-350925	19492	ESO 366-G11
(F20O)	0718229+522156	20622	CGCG 261-043
L333O	0806112-031658	22748	CGCG 003-009
L336O	0819021+211122	23319	UGC 4329
L345O	0832574-225403	23977	ESO 495-G17
L350P	0839329-082901	1003139	

Table 3a.2. Detected objects
– identifications and coordinates - *continued*

Number	2MASS hhmmss.s+ddmmss (J2000.0)	PGC	others
L352O	0843157-203945	24489	ESO 563-G16
L358O	0856563-203138	25141	ESO 563-G34
L360O	0900144+354352	25281	NGC 2719
L364O	0904337+451730	25472	UGC 4753
L371O	0917317+415932	26238	NGC 2799
L376O	0923370-102610	26609	NGC 2863
L378O	0927073+423416	26802	CGCG 210-009
(F26O)	0943288-052156	27825	MCG -01-25-033
L392O	0945031-042947	90940	FGC 936
L393O	0949571-120548	28278	MCG -02-25-019
L401P	1010413-074003	1015078	
L403O	1014436-204836	29894	ESO 567-G28
L410O	1023459+123349	30463	NGC 3230
L416O	1028024-231522	30800	ESO 500-G44
L418O	1031450+464018	31083	UGC 5714
L428O	1043353-100923	31978	MCG -02-28-002
L430O	1046572+595452	32204	UGC 5879
L436O	1055232-073912	32817	MCG -01-28-006
L445O	1109530-234350	33860	IC 2627
L447O	1117402+380309	34497	UGC 6307
L455O	1128100+165531	35292	NGC 3691
(F30O)	1131115+514154	35506	UGC 6505
L459O	1137500+475255	36008	NGC 3769A
L460O	1138215-162630	36049	MCG -03-30-004
(F31O)	1142275-074626	36353	MCG -01-30-025
L468O	1143297-122422	36422	MCG -02-30-025
L474O	1152308-035225	37196	IC 2969
L479P	1155252-101703	170181	
L481O	1156249-121000	37518	MCG -02-31-002
L486O	1200190+503910	37832	UGC 6992
L487O	1201107-011750	37914	UGC 7000
L497O	1212205+291240	38897	NGC 4173
L502P	1216418-251505	781011	
L512O	1222290-043904	40092	IC 784
L535P	1244398-052619	1044733	
L541O	1246148-132141	43071	MCG -02-33-006
L546O	1249423-043447	43385	NGC 4678
L548O	1250345-093111	43465	MCG -01-33-022
L549P	1251090-035539	158144	
L552O	1253365-120104	43800	MCG -02-33-043
L560O	1308377+540428	45561	UGC 8231
L561P	1309167-165311	892101	
L565O	1312520+403237	45889	CGCG 217-018
L568O	1316132+360446	46189	UGC 8341
L569O	1316562-163534	46256	MCG -03-34-040
L572O	1321499-131230	46664	NGC 5105
L582O	1332473+415155	47679	NGC 5214A
L586O	1337410-150615	48144	MCG -02-35-009
(F38O)	1343301+432747	48621	UGC 8688
L597O	1349077-280016	49031	ESO 445-G48
L598O	1351472+505843	49215	IC 0951
(F39N)	1352370-304134		
L606P	1358022-341310	89802	
(F40O)	1405000-145111	50209	MCG -02-36-013
L614O	1406396-311249	50329	ESO 446-G9
L615O	1407054-311243	50360	ESO 446-G12
L633O	1430313+404929	51839	UGC 9337
L634O	1433205+261229	52012	KUG 1431+264
L639O	1443558-182902	52612	ESO 580-G14
L640N	1445115-344405		
(F44N)	1445157-000935		
L641O	1446510-315546	52775	ESO 447-G35
L643O	1447561-141658	52853	MCG -02-38-015
L647O	1456333-243007	53412	ESO 513-G9
L648O	1502261-254847	53700	ESO 513-G14
L654P	1520526-285913	160462	
L656O	1526429+462639	55112	MCG +08-28-032
L661N	1540507-342101		
(L668O)	1602345-254823	56802	ESO 516-G2
L670O	1603469-224417	56889	ESO 516-G5
L688O	1650234+555018	59093	UGC 10589
L692N	1653219-161713		
L705O	1719223+490202	60073	VV 010b

Table 3a.3. Detected objects
– identifications and coordinates - *continued*

Number	2MASS hhmmss.s+ddmmss (J2000.0)	PGC	others
L722O	1842201+460618	62282	CGCG 255-010
L726O	1900033+432620	62661	CGCG 229-012
L727O	1907080+414449	62784	CGCG 229-017
(L734O)	1933188-330857	63352	ESO 398-G8
L735O	1937276-172718	63425	ESO 594-G8
L736O	1940424-221613	63511	ESO 594-G11
L738O	1948132-233029	63678	ESO 526-G6
L740O	1957362-001406	63868	CGCG 372-002
L745O	2017027-120651	64414	MCG -02-51-007
L746O	2018231-272726	64448	ESO 462-G7
L752O	2042431-024601	91678	FGC 2286
L755O	2048122-035221	65413	MCG -01-53-009
L758O	2055067-310530	65707	ESO 463-IG34
L765O	2136162-224404	92680	FGCE 1622
L766O	2145578-344857	67310	ESO 403-G23
L767O	2158057-075042	140989	GSC 5802 00065
(F54N)	2158162-030328		
L777P	2216009-095612	984498	
L780O	2219384-251956	68576	ESO 533-G13
L781O	2221508+425704	68645	UGC 11999
L783O	2223055-285716	68718	NGC 7259
(F56O)	2238204-130808	69381	MCG -02-57-026
L788O	2229599-050657	68996	IC 1447
L794O	2244347-225930	69635	ESO 534-G21
L833O	2356097-272800	72933	ESO 471-G44

Note: No: Source names in brackets are not found in later versions of the public 2MASS database (see Sect. 2).

Table 3b.1. Detected objects – basic data

No	K_{20}	$J - K$	μ_{K5}	b/a	r_{K20}	B_{T_c}	D_{25}	$\mu_{B_{25}}$	T	rms	I_{HI}	V_{HI}	$\sigma_{V_{HI}}$	V_{opt}	W_{50}	W_{20}	D	M_{HI}	L_K	L_B	$\frac{M_{HI}}{L_K}$	$\frac{M_{HI}}{L_B}$
	mag	mag	$\frac{mag}{''}$	"	mag	'	$\frac{mag}{''}$		mJy	$\frac{Jy km}{s}$	$\frac{km}{s}$	$\frac{km}{s}$	$\frac{km}{s}$	$\frac{km}{s}$	$\frac{km}{s}$	Mpc	M_\odot	$L_{\odot, K}$	$L_{\odot, B}$	solar units		
L6O	9.91	0.47	18.87	0.93	48.4	11.01	7.46	24.18	SBd	2.0	66.2	467	0.2	156	176	4.3	8.47	8.64	9.05	0.67	0.26	
L8O	11.56	0.73	18.36	0.57	26.8	13.92	1.07	22.94	SBc	3.6	3.9	6111	9	6108	190	219	80.4	9.77	10.52	10.43	0.18	0.22
L9O	11.52	0.81	18.75	0.58	20.2	13.60	1.52	23.36	Sab	1.5	2.8	3709	4	3725	283	298	50.6	9.23	10.13	10.16	0.12	0.12
L17O	12.14	0.63	18.35	0.62	21.6	14.19	0.90	22.81	Sc	2.7	3.2	7264	7	7242	276	294	98.2	9.86	10.46	10.50	0.25	0.23
(F2O)	13.35	0.81	19.35	0.62	14.9	14.59	0.99	23.48	Sbc	2.4	3.6	3550	4	120	141	47.1	9.27	9.34	9.70	0.85	0.37	
L29O	12.70	0.63	18.87	0.45	39.0	14.82	0.92	23.45	Sc	2.7	2.7	9572	6	9618	187:	213:	125.8	10.00	10.45	10.46	0.36	0.35
L39O	11.76	0.57	18.13	0.78	21.2	14.57	1.10	23.74	Scd	2.1	1.3	5198	8	5141	181	190	69.8	9.17	10.32	10.05	0.07	0.13
L45O	12.38	0.71	18.62	0.30	23.4	13.83	1.33	23.27	Sc	1.7	4.3	5731	10	5693	283	360	75.1	9.76	10.13	10.41	0.42	0.22
L52O	11.54	0.59	18.29	0.61	31.6	14.03	1.18	23.28	SBc	3.0	3.4	6048	4	87	102	82.4	9.74	10.55	10.41	0.15	0.21	
L53O	12.18	0.84	18.24	0.19	26.8	14.98	1.00	24.26	Sd	3.2	2.5	5334	5	5354	289	299	72.5	9.49	10.18	9.92	0.20	0.37
L57O	13.03	0.88	19.04	0.16	22.8	14.49	1.38	23.92	Scd	3.4	2.4	5240	9	5218	266	276	69.1	9.43	9.80	10.07	0.43	0.23
L59O	12.24	0.58	18.09	0.30	23.0	14.76	1.20	23.85	Sbc	5.5	7.0	14251	8	164	205	189.6	10.77	10.99	10.84	0.61	0.85	
L61O	13.01	0.67	18.79	0.23	20.6	14.02	1.19	23.06	Sc	1.8	2.7	5974	9	254	288	81.2	9.62	9.95	10.40	0.47	0.17	
L62O	12.38	0.64	18.21	0.24	21.2	14.88	1.02	23.65	Sb	2.5	3.9	5751	8	5835	250	290	76.8	9.73	10.15	10.01	0.38	0.53
L70O	12.23	0.63	18.41	0.36	25.2	13.68	1.52	23.32	SBbc	2.7	13.2	3914	7	4081	508	594	51.9	9.92	9.87	10.15	1.13	0.59
L78O	11.41	0.60	18.27	0.78	22.8	14.12	1.11	23.13	Sm	2.1	1.2	1914	8	1952	113	128	23.7	8.20	9.52	9.29	0.05	0.08
L84O	11.90	0.73	18.03	0.29	26.4	13.98	1.20	23.12	Sd	1.7	3.3	4787	6	4741	271	292	61.5	9.47	10.15	10.18	0.21	0.19
L86O	12.10	0.62	18.09	0.55	20.6	14.24	1.03	23.14	Irr	1.5	3.3	4977	8	5342	270	339	66.2	9.53	10.14	10.14	0.25	0.25
L87O	11.93	0.65	18.17	0.63	23.4	14.01	1.07	22.99	Sb	2.8	1.7	4517	18	4584	120	200	59.1	9.15	10.10	10.13	0.11	0.10
L91O	12.10	0.66	18.15	0.40	21.8	14.01	1.07	22.93	Sbc	2.2	2.5	2405	12	2474	90	200	32.3	8.79	9.51	9.61	0.19	0.15
L93O	11.50	0.62	18.23	0.82	23.6	13.88	1.25	23.22	Sc	3.1	3.6	4714	7	4719	174	203	60.2	9.49	10.29	10.20	0.16	0.19
L99O	12.25	0.63	18.24	0.25	23.6	14.57	1.22	23.95	SBbc	7.1	5.7	5567	19	5605	225	290	73.2	9.86	10.16	10.09	0.50	0.58
L117O	11.95	0.60	18.09	0.52	22.4	14.10	1.24	23.42	SBC	2.8	2.7	4755	7	4511	165	182	62.9	9.40	10.15	10.15	0.18	0.18
L120N	12.16	0.71	18.08	0.20	21.6					1.8	2.3	4902	10	238	275	66.4	9.38	10.11		0.18		
(L125O)	10.46	0.71	18.55	0.59	40.0	13.90	1.69	24.10	S0	1.3	4.0	5733	4	582	593	75.2	9.73	10.90	10.38	0.07	0.22	
L137O	12.35	0.72	18.57	0.60	24.8	14.47	1.04	23.47	SBc	2.5	4.5	4572	2	4609	61	81	60.0	9.58	9.95	9.96	0.43	0.43
L138O	11.79	0.48	18.12	0.69	21.6	13.62	1.67	23.48	SBc	5.0	5.4	4983	8	4745	276	294	68.6	9.78	10.29	10.42	0.31	0.23
L144P	12.06	0.72	18.14	0.64	20.2	15.04	0.79	23.37	SBab	3.1	10.4	8511	6	7031	235	295	115.9	10.52	10.64	10.31	0.76	1.63
L157O	12.22	0.69	18.35	0.82	28.2	14.10	1.29	23.59	SBd	2.1	9.2	2544	1	2728	130	147	50.3	9.40	9.51	9.61	0.78	0.61
L169O	11.66	0.61	18.05	0.82	20.4	14.55	0.77	22.95	SBc	2.7	1.0	9410	7	9476	56	75	125.4	9.57	10.86	10.57	0.05	0.10
L170O	11.53	0.54	18.24	0.68	29.8	13.51	1.23	22.84	SBc	3.8	4.6	1501	9	1478	151	206	17.9	8.54	9.22	9.29	0.21	0.18
L181O	11.16	0.93	19.18	0.63	26.4	14.52	1.50	24.28	Scd	1.2	9.3	3932	1	3867	142	158	55.4	9.83	10.36	9.87	0.30	0.91
L182O	12.15	0.76	19.70	0.22	38.9	13.85	2.23	24.72	SBcd	1.5	15.2	2801	1	215	239	39.0	9.74	9.65	9.83	1.20	0.80	
L184O	12.58	0.81	19.36	0.38	23.0	14.25	1.13	24.14	S0	1.9	6.5	8523	4	290	322	115.6	10.31	10.43	10.62	0.77	0.49	
(L191O)	11.28	0.71	18.22	0.77	30.6	13.82	1.31	23.28	S0-a	2.4	1.9	1504	11	1502	190	219	19.9	8.25	9.42	9.26	0.07	0.10
(L192O)	12.26	0.59	18.66	0.58	29.8	14.27	1.15	23.43	SBc	2.5	1.9	1665	6	1744	70	96	24.3	8.42	9.20	9.26	0.17	0.15
L198O	11.91	0.78	18.54	0.48	29.4	13.88	1.42	23.35	SBc	2.0	1.2	1595	5	1591	136	144	20.4	8.07	9.19	9.26	0.08	0.06

Table 3b.2. Detected objects – basic data - *continued*

No	K_{20}	$J - K$	μ_{K5}	b/a	r_{K20}	B_{T_c}	D_{25}	$\mu_{B_{25}}$	T	rms	I_{HI}	V_{HI}	$\sigma_{V_{HI}}$	V_{opt}	W_{50}	W_{20}	D	M_{HI}	L_K	L_B	$\frac{M_{HI}}{L_K}$	$\frac{M_{HI}}{L_B}$
	mag	mag	$\frac{mag}{m^2}$	"	mag	'	$\frac{mag}{m^2}$			mJy	$Jy km$	km	km	km	km	km	Mpc	[log] M_\odot	[log] $L_{\odot, K}$	[log] $L_{\odot, B}$	solar units	
L203O	12.21	0.65	18.30	0.69	20.4	15.14	0.87	23.68	E-S0	1.5	0.7	1683	9	1621	60	93	23.1	7.94	9.18	8.86	0.06	0.12
L204O	12.19	0.59	18.41	0.28	21.4	13.44	1.60	23.17	SBbc	3.1	3.0	1697	5	1586	146	162	23.9	8.61	9.21	9.57	0.25	0.11
L211O	12.54	0.74	18.39	0.20	22.2	14.83	1.02	23.52	Sc	2.3	6.9	4219	3		273	291	55.5	9.70	9.81	9.75	0.78	0.89
L214O	11.01	0.63	18.17	0.81	31.8	13.98	1.35	23.44	SBc	2.3	4.6	4100	5	4083	155	205	56.7	9.54	10.44	10.11	0.13	0.27
L215O	11.19	0.69	18.22	0.88	24.8	13.98	0.97	23.30	Sd	2.4	3.1	3715	6		130	167	48.4	9.23	10.23	9.97	0.10	0.18
L219O	12.46	0.63	18.66	0.46	23.8	14.43	1.15	23.56	SBc	2.6	2.2	2552	6	2480	188	200	32.8	8.75	9.38	9.45	0.23	0.20
L220O	12.17	0.68	18.44	0.60	21.6	14.12	1.27	23.72	Sd	1.2	4.6	4917	3		235	260	63.7	9.64	10.07	10.15	0.37	0.31
L223O	12.36	0.55	18.41	0.42	22.2	14.36	1.41	23.82	S0-a	2.7	4.8	1490	4		79	130	19.9	8.65	8.99	9.05	0.46	0.40
L225O	12.05	0.68	18.04	0.36	20.8	14.96	1.02	24.10		1.4	3.2	8254	5		298	321	113.7	9.99	10.62	10.32	0.23	0.47
L226O	11.43	0.68	18.12	0.65	24.2	13.97	1.29	23.34	SBbc	2.5	2.6	5639	6	5608	158	177	74.1	9.53	10.50	10.34	0.11	0.15
L237O	12.03	0.58	18.29	0.49	21.2	13.80	1.15	22.94	Irr	2.6	3.8	944	3	920	55	91	12.1	8.12	8.69	8.84	0.27	0.19
L243O	12.36	0.54	18.49	0.60	20.6	14.63	0.80	23.17		2.3	1.9	4445	7		154	171	56.8	9.16	9.90	9.85	0.18	0.20
L244O	12.07	0.61	18.30	0.44	22.2	14.24	1.09	23.38	SBc	2.4	3.3	4449	4	4422	135	156	58.7	9.43	10.04	10.03	0.24	0.25
L252O	11.95	0.70	18.02	0.64	22.6	14.37	1.19	23.62	SBbc	1.6	5.9	4304	2	4300	228	244	60.3	9.70	10.11	10.00	0.39	0.50
L255O	12.61	0.82	18.64	0.26	23.6	13.82	1.48	23.52	Sc	1.7	4.5	4187	2		250	262	55.5	9.51	9.78	10.15	0.55	0.23
L256O	11.19	0.66	18.22	0.61	33.1	13.51	1.43	23.92	SBc	2.4	4.4	4865	4	17880	227	246	63.3	9.62	10.46	10.39	0.14	0.17
L260O	11.60	0.56	18.19	0.76	20.2	14.04	1.05	22.94	Sc	2.0	1.6	6239	5		92	110	84.2	9.43	10.54	10.43	0.08	0.10
L261O	11.97	0.64	18.13	0.43	24.6	13.77	1.23	23.72	Sd	4.7	10.8	3337	5	3315	173	203	41.6	9.64	9.78	9.92	0.73	0.53
(L270O)	11.76	1.48	18.10	0.47	24.8	13.56	1.48	23.16	SBc	2.4	7.0	6974	4		405	426	94.3	10.17	10.58	10.72	0.39	0.28
L272O	11.84	0.61	18.17	0.54	21.8	13.66	1.18	22.89	SBbc	5.2	8.2	5798	—	5779	264	—	75.2	10.04	10.35	10.48	0.49	0.36
F16O	13.06	0.72	19.02	0.52	15.6	14.00	1.17	23.17	Sb	2.1	3.6	543	10		72	104	6.9	7.60	7.78	8.26	0.66	0.22
(F17O)	12.84	0.72	18.58	0.46	15.1	14.01	1.00	22.90	Sbc	1.0	1.1	1616	2		76	121	23.3	8.15	9.13	9.32	0.10	0.07
L289O	12.47	0.63	18.24	0.44	21.2	13.64				2.3	3.7	912	3	878	94	120	10.4	7.98	8.38	8.77	0.39	0.16
L296P	12.74	0.76	18.83	0.39	21.4	15.94	0.49	24.13		2.5	2.4	6482	11		262	297	83.8	9.60	10.08	9.66	0.33	0.86
L297O	12.60	0.99	18.27	0.20	21.2		0.93		Scd	4.3	4.1	9055	6		320	333	123.6	10.17	10.48		0.49	
(F18N)	13.04	0.74	18.84	0.48	13.8					1.8	1.2	4950	7		83	105	66.4	9.10	9.76		0.22	
L301O	11.80	0.77	18.23	0.74	22.8	13.45	1.31	23.66	Sd	2.7	22.0	2821	2		215	254	35.4	9.81	9.71	9.91	1.27	0.80
L302O	12.80	0.85	18.53	0.16	25.0	15.47	1.45	25.19	S0-a	2.9	9.8	2715	4	2892	303	350	39.2	9.55	9.40	9.19	1.42	2.29
L303O	11.65	0.63	18.13	0.53	26.6	14.01	1.21	23.35	SBc	2.6	5.2	6821	5		236	255	93.5	10.03	10.62	10.53	0.26	0.32
L304N	11.44	0.94	18.24	0.12	48.3					2.7	5.0	2914	3		281	293	38.6	9.24	9.93		0.21	
L308O	11.80	0.61	18.12	0.37	25.2	14.34	0.96	23.37	S0-a	1.9	2.5	8544	8		267	287	115.7	9.90	10.74	10.58	0.14	0.21
(F20O)	12.69	0.91	19.35	0.44	21.9	15.36	0.86	24.11		2.4	3.1	5617	7	5601	106	155	78.1	9.65	10.04	9.83	0.41	0.66
L333O	12.35	0.68	18.69	0.49	30.4	14.17	0.95	22.90	Sd	2.6	3.3	1348	5	1335	64	97	19.5	8.47	8.97	9.10	0.31	0.23
L336O	12.96	0.66	19.08	0.32	29.7	13.95	1.69	24.06	Sc	1.8	6.8	4096	4		218	258	51.5	9.63	9.57	10.03	1.14	0.39
L345O	12.09	0.54	18.49	0.39	21.8	13.68	1.46	23.53	Sb	1.6	3.2	1476	5		201	233	18.2	8.40	9.02	9.24	0.24	0.14

Table 3b.3. Detected objects – basic data - *continued*

No	K_{20}	$J - K$	μ_{K5}	b/a	r_{K20}	B_{T_c}	D_{25}	$\mu_{B_{25}}$	T	rms	I_{HI}	V_{HI}	$\sigma_{V_{HI}}$	V_{opt}	W_{50}	W_{20}	D	M_{HI}	L_K	L_B	$\frac{M_{HI}}{L_K}$	$\frac{M_{HI}}{L_B}$
	mag	mag	$\frac{mag}{''''^2}$	"	mag	'	$\frac{mag}{''''^2}$		mJy	$Jy km$	km	km	km	km	km	Mpc	M_{\odot}	[log]	[log]	[log]	solar units	
L350P	12.79	0.59	18.48	0.33	22.2	15.14	0.93	23.86		1.8	1.5	4316	15	194	260	60.0	9.10	9.77	9.69	0.21	0.26	
L352O	11.51	0.85	18.85	0.64	28.8	12.39	2.25	23.42	SBm	2.3	16.4	1732	1	1603	184	207	22.7	9.30	9.44	9.95	0.72	0.23
L358O	11.93	0.71	18.04	0.35	25.4	13.27	1.22	23.14	Sab	4.4	7.7	2620	6	2558	96	159	31.8	9.26	9.57	9.89	0.50	0.24
L360O	13.58	0.58	19.29	0.10	26.3	12.43	1.26	21.70	Irr	2.3	9.3	3077	4		211	262	42.5	9.60	9.16	10.48	2.75	0.13
L364O	12.75	0.61	18.96	0.18	26.8	14.40	1.69	24.22	Scd	1.3	2.1	1828	3		159	178	24.7	8.48	9.01	9.22	0.29	0.18
L371O	11.91	0.57	18.43	0.35	27.8	12.92	1.83	22.95	SBd	1.4	9.1	1673	4	1859	156	309	20.2	8.94	9.18	9.63	0.58	0.20
L376O	12.01	0.59	18.56	0.60	30.6	12.96	1.05	21.97	Sm	3.4	4.2	1713	7		91	137	23.5	8.74	9.27	9.75	0.29	0.10
L378O	11.87	0.66	18.43	0.73	22.4	15.15	0.81	23.55	Sbc	1.9	1.4	8307	7	8269	97	130	110.9	9.61	10.68	10.22	0.09	0.24
(F26O)	12.97	0.79	19.19	0.60	12.8	13.63	1.35	23.28	SBcd	1.5	11.0	1894	1		117	152	23.6	9.16	10.23	9.49	0.08	0.47
L392O	12.62	1.02	18.27	0.20	21.6					2.8	1.2	6363	—		82	—	82.6	9.30	10.12		0.15	
L393O	12.73	0.80	18.73	0.22	25.0	14.66	0.76	22.90	Sd	2.3	4.9	2580	9		193	274	32.5	9.09	9.26	9.35	0.67	0.55
L401P	12.62	0.85	18.82	0.17	39.6	17.68	0.24	23.48		1.9	2.6	6635	—		127	—	86.7	9.66	10.16	9.00	0.32	4.65
L403O	12.40	0.69	18.32	0.47	20.2	14.21	1.20	23.45	Sbc	1.2	2.9	3728	4		204	243	48.9	9.21	9.75	9.88	0.29	0.21
L410O	9.80	0.80	18.56	0.28	80.0	13.72	2.11	24.23	S0	2.0	1.7	3135	11		191	221	40.0	8.80	10.62	9.91	0.02	0.08
L416O	11.47	0.60	18.03	0.84	23.6	13.54	1.17	22.84	SBc	2.2	4.6	3835	3		123	141	48.4	9.41	10.12	10.14	0.20	0.18
L418O	12.12	0.62	18.47	0.90	21.2	15.04	0.91	23.68	SBc	2.3	4.1	7436	5	7454	231	252	96.0	9.95	10.45	10.14	0.32	0.64
L428O	12.30	0.70	18.49	0.70	20.4	14.36	0.87	22.94	Sc	2.2	1.9	4727	6	4764	222	238	60.6	9.22	9.98	10.01	0.17	0.16
L430O	12.41	0.68	18.47	0.16	22.6	14.18	1.40	23.55	Scd	2.8	5.5	5612	5	5614	278	297	75.8	9.87	10.13	10.28	0.55	0.39
L436O	12.00	0.72	18.02	0.92	21.2	14.86	0.81	23.30	SBd	2.2	2.5	7972	10	8249	132	188	107.7	9.83	10.60	10.31	0.17	0.33
L445O	9.56	0.44	18.11	0.80	50.5	11.93	2.56	23.23	SBc	1.6	10.8	2087	5		50	71	28.9	9.33	10.43	10.34	0.08	0.10
L447O	11.99	0.56	18.01	0.40	20.6	13.57	1.40	23.01	Sd	2.2	7.5	1906	5		207	266	24.6	9.03	9.31	9.55	0.52	0.30
L455O	11.02	0.67	19.17	0.46	42.5	12.57	1.36	22.08	SBb	2.7	2.9	987	11		125	202	10.6	7.88	8.97	9.21	0.08	0.57
(F30O)	13.18	0.87	19.10	0.64	16.5	15.75	0.76	23.95	SBcd	2.0	1.6	6926	8		124	160	93.0	9.51	10.00	9.83	0.33	0.48
L459O	12.92	0.60	19.00	0.28	23.2	14.15	0.99	22.89	SBm	1.5	35.0	734	4	767	229	258	8.8	8.81	8.06	8.43	5.65	2.42
L460O	12.51	0.60	18.33	0.44	21.8	14.30	1.00	23.25	S0-a	1.2	1.6	3793	3	3824	80	104	51.7	9.00	9.76	9.90	0.18	0.13
(F31O)	11.53	0.98	18.53	0.66	29.5	13.69	0.95	22.62	Sc	2.0	2.2	3111	6	3082	109	131	40.0	8.92	9.92	9.92	0.10	0.10
L468O	12.34	0.64	18.74	0.43	22.8	14.25	1.22	23.46	Sc	2.6	2.1	4190	12	4187	204	222	52.8	9.14	9.84	9.94	0.20	0.16
L474O	11.55	0.50	18.42	0.60	29.8	13.01	1.24	22.28	Sbc	3.5	3.6	1620	6	1559	108	142	20.6	8.56	9.34	9.62	0.16	0.09
L479P	12.45	0.60	18.22	0.28	20.2	15.21			Irr	2.1	3.0	3572	6	3557	180	212	44.5	9.15	9.65	9.40	0.31	0.56
L481Oa	12.47	0.76	18.54	0.36	23.0	14.20	1.20	23.46	Sc	1.8	2.5	5423	10		283	318	72.5	9.49	10.06	10.23	0.27	0.18
L481Ob										4.2	5.8	12020	4		99:	121:	158.6	10.54	10.74	10.91	0.62	0.42
L486O	11.66	0.61	18.47	0.56	21.2	13.99	1.37	23.44	Sd	2.5	2.0	752	10	758	124	162	10.4	7.71	8.70	8.63	0.10	0.12
L487O	12.43	0.56	18.66	0.53	22.2	13.98	1.02	22.89	Irr	2.5	6.1	1492	2	1489	80	107	17.4	8.64	8.84	9.08	0.63	0.36
L497Oa	13.11	0.70	19.66	0.18	27.3	12.48	4.02	24.2	Sed	2.4	27.6	1120	0.5	1116	160	178	15.9	9.22	8.49	9.60	5.31	0.41
L497Ob										2.1	7.0	3816	4	1116	424	450	52.5	9.66	9.53	10.64	1.35	0.10
L502Pa	12.48	0.47	18.45	0.61	20.6	15.76	0.52	23.49		2.2	1.1	527	6		64	83	4.1	6.63	7.56	7.11	0.12	0.34
L502Pb										2.2	1.6	5697	14		81	159	74.2	9.32	10.08	9.63	0.17	0.49

Table 3b.4. Detected objects – basic data - *continued*

No	K_{20}	$J - K$	μ_{K5}	b/a	r_{K20}	B_{Tc}	D_{25}	$\mu_{B_{25}}$	T	rms	I_{HI}	V_{HI}	$\sigma_{V_{HI}}$	V_{opt}	W_{50}	W_{20}	D	M_{HI} [log]	L_K [log]	L_B [log]	$\frac{M_{HI}}{L_K}$	$\frac{M_{HI}}{L_B}$
	mag	mag	$\frac{mag}{m^2}$	"	mag	'	$\frac{mag}{m^2}$		mJy	$\frac{Jy km}{s}$	$\frac{km}{s}$	$\frac{km}{s}$	$\frac{km}{s}$	$\frac{km}{s}$	$\frac{km}{s}$	Mpc	M_\odot	$L_{\odot,K}$	$L_{\odot,B}$	solar units		
L512O	11.15	0.73	18.10	0.35	40.2	12.88	1.97	23.25	Sbc	1.0	9.2	4872	2	387	406	65.8	9.97	10.51	10.68	0.29	0.20	
L535P	12.21	0.67	18.17	0.34	21.2	15.74	0.95	24.49		1.7	8.5	1425	1	125	139	16.2	8.72	8.87	8.32	0.72	2.54	
L541O	12.53	0.65	18.63	0.28	21.4	14.29	1.01	23.26	SBcd	1.9	3.6	4952	8	4990	219	269	64.7	9.55	9.94	10.10	0.41	0.28
L546O	12.89	0.53	18.71	0.41	21.8	14.23	0.94	22.95	Sbc	3.5	10.4	1420	2	1433	108	139	18.7	8.93	8.72	9.04	1.63	0.77
L548O	12.07	0.70	18.20	0.33	21.8	14.29	1.24	23.60	Scd	2.4	4.0	4695	6	269	288	59.9	9.53	10.06	10.03	0.29	0.31	
L549P	12.34	0.73	18.10	0.22	22.0	15.70	1.04	24.66		1.5	2.3	6852	7	219	341	89.7	9.64	10.30	9.82	0.22	0.66	
L552O	12.07	0.69	18.36	0.66	20.2	14.68	0.94	23.50	SBc	1.3	0.8	4091	5	4123	127	138	56.6	8.78	10.01	9.83	0.06	0.09
L560O	12.80	0.45	18.69	0.52	22.4	13.44	1.57	23.19	SBbc	3.0	8.2	2470	3	2465	211	232	30.1	9.24	9.17	9.77	1.19	0.30
L561P	13.11	0.83	18.89	0.24	20.6	16.08	0.81	24.69		2.2	4.0	2839	3	179	194	36.8	9.11	9.22	8.89	0.77	1.64	
L565O	12.62	0.54	18.89	0.68	23.0	15.04	0.55	22.52		1.2	3.2	562	1	591	68	90	4.7	7.22	7.62	7.52	0.39	0.50
L568O	11.95	0.71	18.34	0.58	21.8	14.68	0.91	23.18	Sc	2.1	2.7	6817	5	318	332	91.5	9.73	10.48	10.24	0.18	0.30	
L569O	12.62	0.63	18.44	0.34	20.2	13.53	1.32	23.09	Scd	3.3	14.8	1738	2	315	335	23.1	9.27	9.01	9.51	1.81	0.58	
L572O	11.48	0.41	19.37	0.39	37.7	12.47	1.92	22.83	Sbc	1.8	9.9	2902	2	214	236	38.2	9.53	9.91	10.37	0.42	0.14	
L582O	12.14	0.92	18.06	0.33	26.0	15.05	0.78	23.22	Sb	2.8	7.6	8186	8	8154	295	350	106.7	10.31	10.53	10.23	0.60	1.21
L586O	11.62	0.80	18.21	0.84	21.2	14.43	1.17	23.76	SBm	1.7	5.4	7990	3	7979	251	272	108.5	10.18	10.76	10.49	0.26	0.48
(F38O)	12.75	0.78	19.07	0.56	19.7	14.36	1.04	23.21	Sd	1.7	5.0	1359	2	1343	60	94	17.1	8.54	8.70	8.92	0.69	0.42
L597O	13.14	0.48	19.30	0.68	21.0	14.66	1.03	23.67	Sbc	2.4	3.6	4881	8	331	347	65.5	9.56	9.71	9.96	0.71	0.40	
L598O	11.29	0.68	18.03	0.86	23.8	14.56	1.10	23.58	SBcd	3.0	6.2	4055	7	4035	120	214	55.9	9.66	10.31	9.86	0.22	0.63
(F39N)	12.55	0.97	18.68	0.82	17.5					1.5	1.7	5387	5	144	166	70.6	9.30	10.01	0.70			
L606P	12.32	0.54	18.22	0.40	22.0	14.70	0.91	23.63		3.3	1.3	541	6	50	69	6.2	7.07	7.98	7.89	0.12	0.15	
(F40O)	13.31	0.78	18.93	0.48	19.3	14.52	0.97	23.63	Sbc	2.5	4.7	4882	6	12500	185	216	67.9	9.71	9.67	10.05	1.09	0.46
L614O	12.25	0.62	18.16	0.47	20.5	13.46	1.22	22.87	Sbc	1.8	4.7	4415	2	199	220	56.8	9.55	9.94	10.32	0.41	0.17	
L615O	11.99	0.61	18.18	0.49	23.6	14.18	0.97	23.06	Sbc	1.5	3.0	4108	6	240	273	52.4	9.29	9.98	9.96	0.21	0.21	
L633O	12.51	0.73	18.79	0.44	20.8	14.82	0.90	23.30	Sbc	2.7	1.8	5450	8	344	354	75.0	9.38	10.08	10.01	0.20	0.23	
L634O	13.26	0.81	18.95	0.32	20.4	14.79	0.84	23.20	Sc	1.5	4.7	4782	3	230	252	64.4	9.66	9.65	9.89	1.03	0.58	
L639O	11.82	0.62	18.01	0.76	24.2	13.88	1.08	23.19	SBcd	2.6	3.3	6080	5	6080	96	127	79.7	9.69	10.41	10.44	0.19	0.18
L640N	12.19	0.48	18.34	0.56	20.4					1.7	1.1	8255	13	114	161	108.2	9.48	10.52	0.09			
(F44N)	13.56	0.72	19.18	0.48	11.3					1.8	1.0	1650	6	76	94	22.4	8.07	8.61	0.29			
L641O	13.23	0.77	19.04	0.24	24.4	14.32	0.94	23.42	Sb	4.6	3.9	11432	11	11401	130	174	152.4	10.33	10.41	10.83	0.84	0.32
L643O	11.77	0.55	18.63	0.55	43.2	13.75	1.78	24.10	SBc	2.7	22.3	1979	2	217	260	24.0	9.48	9.39	9.45	1.25	1.06	
L647Oa	11.79	0.53	18.06	0.67	20.6	13.16	1.11	22.76	Sc	2.3	3.1	6896	8	6815	270	300	91.9	9.79	10.54	10.85	0.18	0.09
L647Ob										2.3	2.0	8563	14	6815	161	213	114.6	9.79	10.73	11.05	0.11	0.05
L648O	12.45	0.79	18.46	0.30	22.2	14.72	0.67	23.47	S0-a	2.5	3.9	11328	4	11140	118	150	152.2	10.33	10.72	10.67	0.41	0.46
L654Pa										2.4	3.5	3953	—	183	—	52.7	9.36	10.04	9.95	0.21	0.26	
L654Pb	11.83	0.93	18.28	0.71	21.0	14.22	0.81	23.78		2.4	1.7	6006	14	182	222	80.5	9.41	10.41	10.31	0.10	0.12	

Table 3b.5. Detected objects – basic data - *continued*

No	K_{20}	$J - K$	μ_{K5}	b/a	r_{K20}	B_{T_c}	D_{25}	$\mu_{B_{25}}$	T	rms	I_{HI}	V_{HI}	$\sigma_{V_{HI}}$	V_{opt}	W_{50}	W_{20}	D	M_{HI}	L_K	L_B	$\frac{M_{HI}}{L_K}$	$\frac{M_{HI}}{L_B}$
	mag	mag	$\frac{mag}{''^2}$	"	mag	'	$\frac{mag}{''^2}$	mJy	$\frac{Jy km}{s}$	$\frac{km}{s}$	$\frac{km}{s}$	$\frac{km}{s}$	$\frac{km}{s}$	$\frac{km}{s}$	Mpc	M_\odot	[log]	[log]	[log]	solar units		
L656O	13.07	0.77	18.83	0.22	21.2	15.12	0.95	23.71	Sc	2.6	2.7	5382	11	213	260	70.8	9.50	9.80	9.84	0.50	0.46	
L661N	13.01	0.62	19.26	0.42	23.4					2.2	1.4	4560	12	97	155	62.1	9.10	9.71		0.25		
L668O	11.83	0.77	18.01	0.45	25.4	14.27	0.91	23.36	SBc	1.9	2.5	7477	6	7431	258	272	100.6	9.78	10.61	10.49	0.15	0.19
L670O	11.24	0.77	18.08	0.59	25.4	14.13	0.76	23.04	Sbc	1.8	2.5	7347	9	368	393	101.3	9.78	10.85	10.55	0.09	0.17	
(L688O)	11.83	0.80	18.42	0.42	35.3	14.83	1.34	24.19	Sd	2.6	5.7	2115	3	2130	229	244	28.0	9.02	9.50	9.16	0.34	0.74
L692N	11.99	0.77	18.48	0.92	22.8					2.8	3.1	7640	—	110	—	102.8	9.89	10.56		0.21		
L705O	11.05	0.86	18.96	0.22	56.3	15.93	0.67	23.89	Sd	2.2	2.6	7438	13	95	199	99.1	9.78	10.90	9.81	0.08	0.92	
L722O	12.45	0.62	18.72	0.56	22.4	15.25	0.84	23.92	SBbc	4.3	2.7	9934	6	58	85	133.8	10.06	10.61	10.34	0.28	0.52	
L726O	11.92	0.70	18.17	0.69	22.6	15.35	0.68	23.63	SBbc	4.0	4.3	8828	3	8826	60	80	118.9	10.16	10.71	10.20	0.28	0.90
L727O	13.21	0.50	18.85	0.37	22.4	14.93	0.86	23.97	SBbc	3.4	0.6	5039	11	5021	144	153	67.9	8.81	9.71	9.88	0.13	0.09
(L734O)	12.04	0.64	18.37	0.43	28.2	13.67	1.15	23.13	Sc	2.4	3.0	5952	14	5933	310	362	79.9	9.65	10.32	10.53	0.22	0.13
L735O	11.98	0.90	18.27	0.29	24.6	13.68	1.46	23.78	Scd	1.5	4.4	6136	4	6130	325	351	81.8	9.84	10.37	10.55	0.30	0.20
L736O	12.36	0.81	18.44	0.37	20.6	13.55	1.00	22.60	Sbc	2.1	2.7	1792	5	83	126	23.0	8.53	9.11	9.49	0.26	0.11	
L738O	12.50	0.75	18.53	0.23	24.0	14.03	1.24	23.60	Sbc	3.5	13.4	6385	6	6398	267	343	87.9	10.39	10.22	10.47	1.47	0.83
L740O	11.95	0.65	18.25	0.61	20.8	14.73	0.79	23.92	Sc	1.9	5.3	6821	6	191	249	90.6	10.01	10.47	10.21	0.35	0.63	
L745O	12.38	0.85	18.19	0.29	20.2	14.68	0.78	23.13	Sb	1.1	5.8	5646	3	349	397	75.6	9.89	10.13	10.08	0.57	0.65	
L746O	12.13	xxx	18.73	0.59	24.8	13.63	1.41	23.31	Sbc	2.6	6.9	6130	7	323	368	82.3	10.04	10.31	10.57	0.54	0.29	
L752O	12.82	0.74	18.69	0.22	20.8		1.51		Scd	2.1	3.7	3783	6	245	272	50.0	9.34	9.60		0.54		
L755O	11.94	0.62	18.30	0.74	20.8					4.1	1.2	6042	8	125	139	81.7	9.28	10.38		0.08		
L758O	12.23	0.63	18.18	0.34	22.6	15.29	0.78	23.94		1.7	13.8	5965	4	5993	220	403	80.7	10.3	10.25	9.89	1.18	2.57
L765O	12.53	0.77	18.32	0.17	22.8	15.29	0.81	23.65	Sc	3.0	2.1	4994	11	172	213	65.9	9.33	9.96	9.71	0.24	0.42	
L766Oa	12.47	0.69	18.32	0.24	20.8	14.01	1.21	23.16	Sc	4.4	4.3	5139	12	229	254	66.6	9.65	9.99	10.24	0.46	0.26	
L766Ob										2.7	3.7	13006	—	100	—	170.4	10.40	10.81	11.05	0.39	0.23	
L767O	11.74	0.49	18.07	0.42	29.2	14.46	1.23	23.77	Sc	2.0	5.5	5248	7	5321	248	302	69.1	9.79	10.32	10.08	0.30	0.50
(F54N)	12.91	1.01	18.87	0.46	17.6					1.5	3.7	2961	2	309	320	39.7	9.14	9.36		0.60		
L777P	12.30	0.51	18.16	0.53	21.0	16.29	0.49	23.73		7.9	9.2	6311	5	154	170	85.2	10.20	10.27	9.54	0.84	4.57	
L780O	12.87	0.60	18.73	0.30	20.6	14.00	0.87	23.54	Sc	4.1	3.0	4738	5	4707	230	238	65.5	9.48	9.82	10.22	0.46	0.18
L781O	12.56	0.61	18.57	0.21	23.2	14.12	0.88	23.70	Sc	2.1	2.0	3287	7	162	179	46.0	9.00	9.63	9.87	0.23	0.13	
L783O	11.21	0.64	18.04	0.67	32.8	13.36	1.20	22.57	Sb	1.9	11.6	1713	1	1718	149	180	23.9	9.19	9.61	9.61	0.39	0.39
(F56O)	13.10	1.18	19.17	0.48	16.2	14.65	1.03	23.70	SBm	6.9	3.5	2692	6	148	162	36.0	9.03	9.21	9.45	0.67	0.38	
L788O	10.77	0.58	18.68	0.49	33.9	12.97	1.42	22.67	Sb	1.5	3.7	2953	3	315	326	41.1	9.17	9.47	10.23	0.50	0.09	
L794O	12.72	0.72	18.92	0.36	26.8	14.56	1.04	23.45	Sc	1.8	2.3	3140	4	3159	187	204	41.7	8.97	9.48	9.61	0.31	0.23
L833O	12.17	0.74	18.20	0.22	24.2	14.09	1.26	23.32	Sab	4.0	2.2	3000	9	2999	222	233	39.8	8.91	9.66	9.76	0.18	0.14

Note: No: source names in brackets are not found in later versions of the public 2MASS database (see Sect. 2).

Table 4a. Marginal detections
– identifications and coordinates

Number	2MASS hhmmss.s+ddmmss (J2000.0)	PGC	others
L20O	0033168-114120	170423	GSC 5271 01985
L88O	0200154-060530	7585	KUG 0157-063
L136O	0242063-005335	10224	UGC 2177
L206O	0342313-160005	13612	MCG -03-10-038
L249O	0443334-274006	15883	ESO 421-G13
L314O	0711574-352518	20373	ESO 367-G4
L342O	0825577-114645	23658	MCG -02-22-012
L400O	1005255-174753	29281	ESO 567-G12
L429O	1046559+464235	32201	KUG 1043+469
L438O	1059336-061646	156112	FGC 1176
L501O	1215127-273937	39175	ESO 505-G28
L579O	1329480-234059	47390	ESO 509-G30
L623O	1414140-185218	50852	ESO 579-G5
L644O	1448271+314730	52874	IC 4509
L646O	1453336+490807	53219	KUG 1451+493
L651O	1506463+125101	53961	CGCG 077-007
L712O	1803021+292225	61320	CGCG 171-049
L739O	1952561-250900	63776	ESO 526-G11
L741O	2002039-273339	64007	ESO 461-G33
L769O	2203532-165049	91725	FGC 2359
L771O	2209116-202838	68158	ESO 601-G24
L773O	2209370-271447	68176	ESO 532-G23
L778O	2218472-032946	68549	MCG -01-56-00

Table 4b. Marginal detections – basic data

No	K_{20}	$J - K$	μ_{K5}	b/a	$r_{K_{20}}$	B_{T_c}	D_{25}	$\mu_{B_{25}}$	T	rms	I_{HI}	V_{HI}	V_{opt}	W_{50}	D	M_{HI}	L_K	L_B	$\frac{M_{HI}}{L_K}$	$\frac{M_{HI}}{L_B}$
	mag	mag	$\frac{mag}{''/2}$		$''$	mag	'	$\frac{mag}{''/2}$		mJy	$\frac{Jy km}{s}$	$\frac{km}{s}$	$\frac{km}{s}$	$\frac{km}{s}$	Mpc	M_\odot	$L_{\odot,K}$	$L_{\odot,B}$		
L20O	11.78	0.73	18.01	0.48	22.6	14.50	0.72	22.68	Sc	2.4	2.2	8072	7992	103	107.6	9.78	10.68	10.46	0.12	0.21
L88O	12.03	0.63	18.16	0.76	20.2	14.63	0.74	22.86	Sc	4.6	2.7	5410	5448	92	73.2	9.54	10.25	10.07	0.19	0.29
L136O	12.56	0.78	18.28	0.20	21.4	14.97	0.98	23.66	Sc	2.7	3.6	3977		66	53.1	9.38	9.76	9.65	0.42	0.53
L206O	12.40	0.63	18.25	0.31	23.4	14.10	1.06	23.25	Sb	3.3	2.4	1573	1555	102	20.5	8.38	9.00	9.18	0.24	0.16
L249Oa	12.11	0.74	18.06	0.31	24.8	14.22	1.22	23.38	Sbc	2.1	2.0	5349		149	72.2	9.39	10.20	10.20	0.15	0.15
L249Ob										3.3	1.7	10652		69	140.2	9.90	10.78	10.80	0.13	0.12
L314O	12.57	0.94	18.55	0.39	20.4	14.53	0.91	24.06	Sbc	4.5	3.7	17205		332	232.5	10.67	11.04	11.11	0.43	0.36
L342O	11.48	0.76	18.20	0.15	41.0	13.04	1.63	22.94	Scd	4.0	2.3	2718		159	34.9	8.82	9.83	10.06	0.10	0.06
L400O	11.24	0.58	18.11	0.41	31.0	14.14	1.09	23.15	Sb	2.4	1.2	3053		279	40.6	8.67	10.05	9.75	0.04	0.08
L429O	13.15	0.44	18.94	0.19	21.2	15.25	0.80	23.47	Sbc	2.1	0.9	2318		114	29.5	8.27	9.01	9.03	0.18	0.17
L438O	12.31	0.81	18.01	0.19	20.2	16.53	0.87	25.09		3.3	2.2	2522		74	30.6	8.69	9.38	8.55	0.20	1.36
L501O	12.26	0.64	18.43	0.52	21.4	14.53	0.74	22.88	SBd	3.3	1.9	7583	7507	152	103.8	9.68	10.46	10.41	0.17	0.19
L579O	12.21	0.67	18.77	0.38	25.6	14.35	1.10	23.50	Sbc	1.4	1.1	5071		232	67.7	9.08	10.11	10.12	0.09	0.09
L623O	12.14	0.64	18.13	0.18	26.2	14.27	0.99	23.23	Sbc	2.0	3.4	8634		390	114.6	10.02	10.59	10.60	0.27	0.26
L644O	12.16	0.60	18.11	0.36	21.6	13.85	0.89	22.32	Sb	3.1	1.9	2868	2885	185	38.4	8.82	9.64	9.82	0.15	0.10
L646O	12.13	0.62	18.14	0.48	21.0	15.28	0.68	23.30	Sc	3.0	3.5	9204	9350	309	123.0	10.10	10.66	10.26	0.27	0.69
L651O	12.24	0.73	18.11	0.38	21.4	15.24	0.69	23.29	Sc	3.7	5.5	6579	6582	42	87.8	10.00	10.32	9.98	0.48	1.04
L712O	11.96	0.74	18.01	0.64	21.0	15.42	0.76	23.85		2.9	3.3	6945	7048	462	94.5	9.84	10.50	9.97	0.22	0.74
L739O	12.40	0.71	18.41	0.23	24.6	14.43	0.98	23.48	Sc	5.5	2.5	5857	5822	286	77.9	9.55	10.16	10.20	0.25	0.22
L741O	11.36	0.68	18.01	0.75	21.6	13.75	0.94	22.76	Sc	3.8	3.3	5916		250	78.8	9.68	10.58	10.48	0.13	0.16
L769O	12.74	0.65	18.82	0.23	30.6	0.00	0.74		Sc	2.7	1.5	4016		166	56.2	9.05	9.73	15.69	0.21	0.00
L771O	12.25	0.66	18.03	0.42	21.6	14.54	0.89	23.23	SBb	3.2	2.1	11061	11280	175	146.4	10.03	10.76	10.71	0.18	0.21
L773O	12.23	0.62	18.49	0.64	21.4	14.25	1.06	23.22	SBbc	4.3	1.4	7398	7252	52	100.8	9.53	10.45	10.50	0.12	0.11
L778O	11.54	0.56	18.09	0.68	23.6	13.77	0.90	22.71	SBd	4.3	2.4	4970	4969	176	64.9	9.38	10.34	10.31	0.11	0.12

Table 5a.1. Undetected objects
– identifications and coordinates

Number	2MASS hhmmss.s+ddmmss (J2000.0)	PGC	others
L4P	0013146+404632	2170755	
L23O	0037092-175743	2219	ESO 540-G5
L36O	0100136-304836	3595	ESO 412-G1
L41P	0106015-060925	1036120	
L46O	0111215-181646	4272	MCG -03-04-25
L49O	0114254-072842	4471	MCG -01-04-16
L50O	0114443+502709	4481	UGC 786
L55O	0117520-361847	4661	ESO 352-G36
L65O	0139339-120438	6141	MCG -02-05-32
L80O	0155289-310618	7176	ESO 414-G10
L92O	0201351-311700	7690	ESO 414-G24
L98O	0206276+133952	1437074	FGC 243
L100O	0207153+461519	90589	FGC 245
L107N	0218006-025823		
L115P	0227117+414120	2185194	
L118O	0228569-222104	9442	NGC 951
L128O	0236123+401210	9883	CGCG 539-59
L131O	0239425-211423	10085	ESO 545-G43
L134P	0241261-033936	1068434	
(F9N)	0256014-141326		
(L147N)	0257331-090552		
L151P	0258245+443942	2249237	
L156P	0303035-115056	145211	
L164N	0309131-141053		
L171P	0315264+410418	2175237	
L173P	0316422+400344	213184	
L176O	0318004+413106	12270	NGC 1264
L180O	0319538-033537	12439	FGC 410
L196O	0334381-172833	13235	ESO 548-G46
L199O	0337432-225436	13381	ESO 482-G17
L200O	0338512-094411	13432	MCG -02-10-3
L207O	0343078-171106	13659	LSBG F549-29
L210P	0346291-111959	967071	
L222P	0358337-111759	967495	
L240P	0431513-293708	133177	
L258P	0458504-110500	178035	
L266O	0507041-182521	16762	MCG -03-13-74
L278N	0539281-004439		
L280N	0541365+513558		
L284P	0545007+494013	2349901	
L286P	0551325-123801	949939	
L288O	0557284-295735	18138	ESO 424-G41
L299O	0614368-302536	18693	ESO 425-G16
L305O	0634277-274248	19269	ESO 426-G24
L306O	0640040-374548	19396	ESO 308-G24
L307O	0641352+501551	19440	CGCG 233-26
L312P	0657029+424635	2205935	
F19N	0709418+503614		
L316O	0720334+490518	20719	CGCG 235-007
(L328O)	0759559+472427	22418	UGC 4136
L347O	0833427-183153	24019	ESO 562-G16
L348O	0837450-191842	24246	ESO 563-G4
L354P	0843518-110808	969541	
L355O	0844225-231255	24544	ESO 496-G5
L359N	0858094-152210		
L365O	0907390+283810	1841518	FGC 842
L374O	0922337+501200	26541	UGC 4975
L382P	0929293-051228	1047805	
L385O	0938552-045128	27515	MCG -01-25-11

Table 5a.2. Undetected objects
– identifications and coordinates - *continued*

Number	2MASS hhmmss.s+ddmmss (J2000.0)	PGC	others
(F25O)	0941462+465826	27693	UGC 5169
L411O	1024175-054040	1041741	FGC 1062
L467O	1143037+404935	36381	UGC 6679
L493O	1204495+321537	91167	FGC 1358
L516O	1228359-222950	41041	ESO 574-G2
L531O	1242007-241750	42623	ESO 507-G1
L536P	1244416-180312	873438	
L573P	1325301-073549	1016275	
L574O	1327562-312910	98330	
L580N	1329480-225220		
L589O	1343410+545707	91308	FGC 1661
L591O	1344498+592525	48726	MCG +10-20-21
L596O	1348567+595012	49016	UGC 8741
L607O	1358550-263247		AM 1356-261
L616P	1407594-342215	89865	
F41O	1409097+534916	50505	MCG +09-23-42
L621O	1413498+574610	50803	MCG +10-20-84
L622O	1414108+210116	50844	CGCG 133-16
L630O	1427322-311417	51628	ESO 447-G5
F43N	1428300-324000		
(L649P)	1502329-025150	1081087	
L657N	1527242-172215		
L666N	1601551-222731		
L669O	1603106+492502	56846	MCG +08-29-40
L671N	1604570-321710		
(L673O)	1608463+164541	57278	CGCG 108-158
L681P	1625543+435127	2230836	
(F46N)	1626318+491051		
L682O	1628587+422511	91536	FGC 2039
L686O	1637275+465005	58624	MCG +08-30-36
(F48O)	1639237+455404	58701	MCG +08-30-44
L687O	1645574+395908	91553	FGC 2067
L689O	1650561+594308	59109	UGC 10590
L691O	1652580+533858	91565	FGC 2082
L699O	1714474+522317	59921	CGCG 277-31
L706P	1727232+121230	1405561	
L707N	1727479+295117		
L708N	1728392+152716		
L733O	1929177-205510	63275	ESO 594-G1
L737O	1941463+503602	63534	CGCG 257-007
L742O	2005378-250842	64077	ESO 527-G8
L744O	2015134-183910	92575	FGCE 1448
L747O	2021261-220721	64521	ESO 596-G20
L751N	2036015-335250		
L753O	2045178-351427	65312	ESO 401-G7
F51O	2047447-264341	65393	ESO 529-G3
L759P	2058016-354925	132331	
L760O	2118531+154101	1490846	UGC 11719
L770O	2208329-183728	68125	ESO 601-G23
L774O	2210507+411525	68221	UGC 11936
L775P	2212462+383404	2130585	
(F55N)	2228158-074356		
(L791O)	2233495-285406	69159	ESO 468-G14
L797O	2249207-145013	91756	FGC 2421
L819P	2320521+432418	2219987	
(F59N)	2334402+440720		
L836P	2359437-290935	132729	

Note: No: Source names in brackets are not found in later versions of the public 2MASS database (see Sect. 2).

Table 5b.1. Undetected objects – basic data

No	K_{20} mag	$J - K$ mag	μ_{K5} $\frac{mag}{''^2}$	b/a	$r_{K_{20}}$ ''	B_{T_c} mag	D_{25} '	$\mu_{B_{25}}$ $\frac{mag}{''^2}$	T	rms mJy	I_{HI} $\frac{Jy km}{s}$	$\frac{M_{HI}}{L_K}$ solar units	$\frac{M_{HI}}{L_B}$ solar units	search mode
L4P	12.61	1.28	18.29	0.30	20.4	16.75	0.58	24.60		5.6	4.2	0.51	3.18	lo
L23O	12.39	0.89	18.54	0.25	20.6	14.42	1.30	23.65	Sb	4.2	3.1	0.31	0.28	lo
L36O	11.78	0.98	18.19	0.70	24.4	14.10	0.92	22.82	Sbc	3.7	2.8	0.16	0.19	lo
L41P	12.24	0.93	18.16	0.40	21.8	15.41	0.78	24.13		3.2	2.4	0.21	0.53	lo
										2.9	2.2	0.19	0.49	hi
L46O	12.97	0.99	18.99	0.51	20.6	15.67	0.63	23.45	S0-a	2.0	1.5	0.26	0.42	lo
L49O	11.87	0.97	18.08	0.69	20.2	14.54	0.88	23.36		4.3	3.2	0.20	0.32	lo
L50O	12.55	1.13	18.42	0.24	21.2	14.72	0.87	23.89	Sc	2.9	2.2	0.25	0.25	lo
L55O	12.84	0.64	18.83	0.32	21.4	14.31	0.96	22.98	Sc	5.5	4.1	0.61	0.33	lo
L65O	11.41	1.08	18.64	0.54	28.6	14.13	1.15	23.28	Sb	6.5	4.9	0.20	0.33	lo
L80O	12.51	1.05	18.29	0.22	20.6	14.41	1.35	23.76	Sc	2.8	2.1	0.23	0.18	lo
L92O	12.98	1.21	18.68	0.23	20.8	15.46	1.04	24.18	Sc	2.6	2.0	0.34	0.46	lo
L98O	13.03	1.08	18.78	0.20	20.2	16.71	0.89	25.57		2.5	1.9	0.33	1.37	lo
L100O	12.17	1.12	18.16	0.24	25.2	14.81	0.82	23.57	Sed	6.2	4.6	0.37	0.59	lo
L107N	10.12	1.29	18.69	0.62	60.0					3.6	2.7	0.03		lo
L115P	12.11	1.02	18.04	0.35	23.8	15.84	0.78	24.29		3.9	3.0	0.23	0.97	lo
L118O	12.74	0.98	18.62	0.26	23.4	14.60	1.04	23.56	SBab	6.3	4.7	0.65	0.49	lo
L128O	12.32	1.73	18.10	0.25	20.6	15.29	1.78	25.53		3.9	2.9	0.27	0.57	lo
L131O	12.30	1.03	18.58	0.49	21.6	14.26	0.89	22.81	Sc	4.2	3.1	0.29	0.23	lo
L134P	12.43	1.14	18.27	0.30	23.2	16.45	0.81	24.88		3.0	2.2	0.23	1.29	lo
(F9N)	12.75	1.00	19.03	0.62	16.5					5.2	3.9	0.54		lo
(L147N)	10.91	1.65	18.21	0.28	60.3					2.8	2.1	0.05		lo
L151P	12.32	0.91	18.34	0.37	22.6	15.21	0.89	24.54		5.2	3.9	0.36	0.72	lo
L156P	12.01	1.07	18.07	0.20	24.4	15.25	1.35	24.93		4.2	3.2	0.22	0.61	lo
L164N	12.52	1.02	18.29	0.23	21.6					2.4	1.8	0.20		lo
L171P	12.54	1.24	18.47	0.29	21.0	16.85	0.72	25.44		5.0	3.8	0.43	3.13	lo
L173P	11.20	1.00	18.63	0.39	46.4	15.44	0.62	24.00		5.0	3.8	0.12	0.86	lo
L176O	11.39	0.98	19.09	0.61	25.8	14.06	0.10	23.57	SBab	3.4	2.6	0.10	0.16	lo
L180O	11.94	0.96	18.09	0.18	31.0	14.10	1.55	23.85	Sc	5.4	4.1	0.27	0.27	lo
L196O	12.92	0.92	18.85	0.54	21.0	15.25	0.87	24.04	Sbc	5.9	4.4	0.71	0.84	lo
L199O	12.19	0.94	18.76	0.55	23.0	14.29	1.29	23.63	Sab	5.1	3.8	0.32	0.30	lo
L200O	12.12	1.01	18.13	0.36	22.0	14.91	0.78	23.42	Sc	3.9	2.9	0.22	0.40	lo
L207O	11.84	0.96	18.37	0.20	33.8	13.63	1.42	23.53	Sd	4.8	3.6	0.22	0.15	lo
L210P	12.02	1.17	18.20	0.50	26.8	15.69	0.72	23.97		2.0	1.5	0.11	0.44	lo
L222P	12.38	1.02	18.15	0.40	20.2	15.46	0.69	23.66		1.9	1.5	0.14	0.34	lo
L240P	12.21	0.99	18.07	0.26	20.2	14.62	0.97	23.32	Sc	3.7	2.8	0.23	0.30	lo
L258P	12.11	1.19	18.20	0.29	21.0	15.25	1.00	24.54		4.5	3.4	0.26	0.67	lo
L266O	12.16	0.94	18.40	0.68	21.8		0.48		Sd	6.0	4.5	0.36		lo
L278N	12.21	1.11	18.19	0.70	21.6					1.9	1.4	0.12		lo
L280N	11.60	1.54	18.48	0.32	37.8					6.9	5.2	0.25		lo
L284P	12.88	0.75	18.76	0.32	20.4	15.34	0.62	24.17		3.1	2.3	0.37	0.49	lo
L286P	12.56	1.08	18.34	0.30	22.8	15.63	0.78	25.05		6.4	4.8	0.56	1.30	lo
L288O	11.73	0.83	18.25	0.60	23.6	14.76	0.93	23.45	Sc	5.3	4.0	0.21	0.48	lo
L299O	11.90	1.08	18.60	0.57	26.2	15.63	0.87	24.21	Sbc	2.8	2.1	0.13	0.57	lo
L305O	12.26	1.35	18.12	0.24	24.8	14.95	1.35	24.48	Sc	4.5	3.4	0.30	0.49	lo
L306O	11.74	1.00	18.43	0.46	31.0	13.70	1.28	23.35	Sab	6.9	5.2	0.28	0.24	lo
L307O	12.98	1.00	18.68	0.27	27.0	14.89	0.77	23.55		3.4	2.6	0.44	0.35	lo
L312P	12.26	1.36	18.12	0.50	22.0	16.38	0.71	24.83		2.7	2.0	0.18	1.08	lo
F19N	12.74	0.84	19.14	0.84	19.1					4.3	3.2	0.44		lo
										8.7	6.5			hi

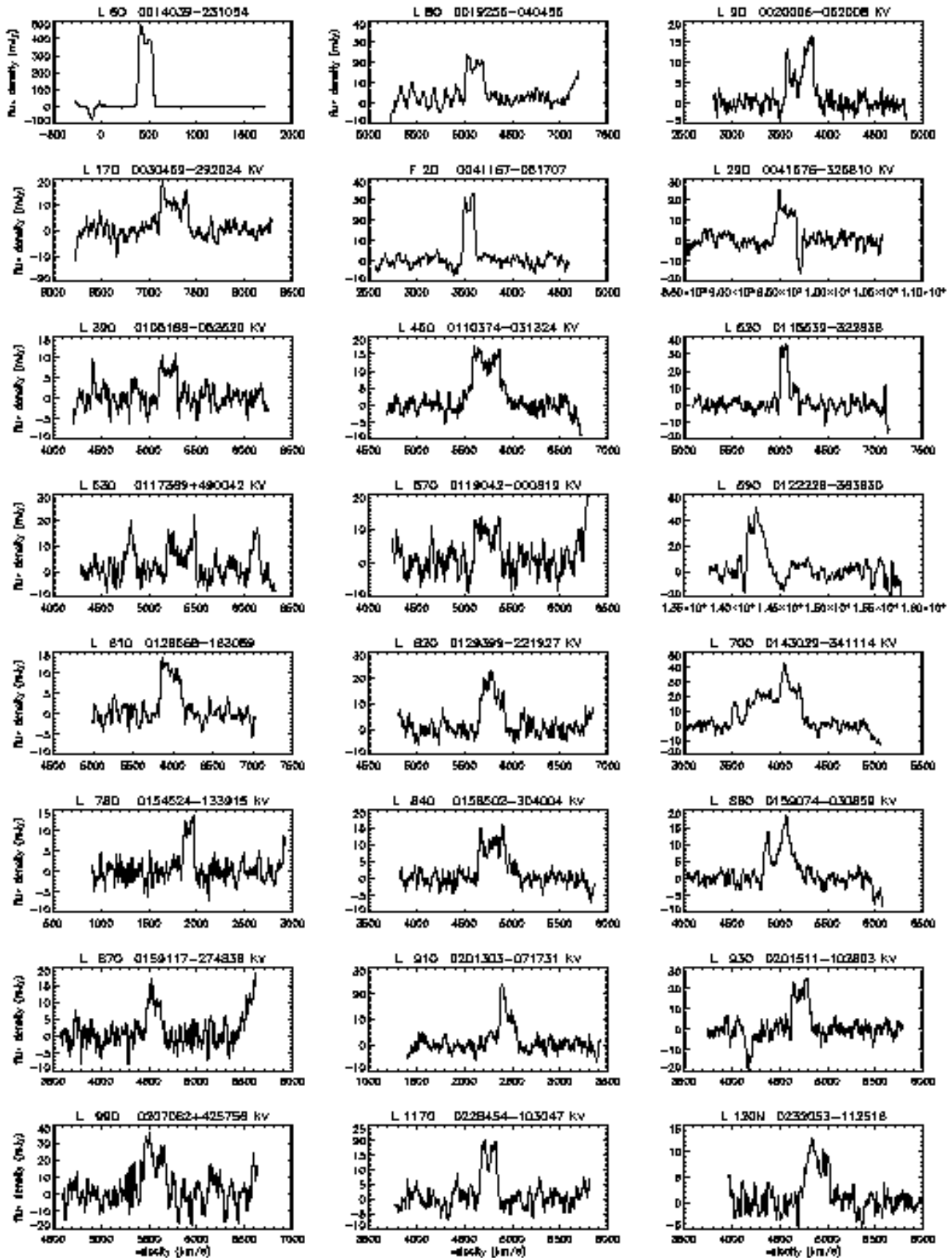
Table 5b.2. Undetected objects – basic data - *continued*

No	K_{20} mag	$J - K$ mag	μ_{K5} $\frac{mag}{''^2}$	b/a	r_{K20} ''	B_{Tc} mag	D_{25} '	μ_{B25} $\frac{mag}{''^2}$	T	rms mJy	I_{HI} $\frac{Jy km}{s}$	$\frac{M_{HI}}{L_K}$ solar units	$\frac{M_{HI}}{L_B}$	search mode
L316O	11.98	1.04	18.19	0.63	20.4	14.86	0.79	23.53	Sd	4.8	3.6	0.25	0.48	lo
(L328O)	11.23	1.07	18.50	0.16	53.4	14.03	1.51	23.80	Sa	4.5	3.4	0.12	0.21	lo
L347O	11.25	0.88	18.56	0.55	41.0	13.07	1.03	22.19	Sbc	6.3	4.7	0.16	0.12	lo
										4.3	3.2	0.11	0.08	hi
L348O	12.37	1.14	18.40	0.21	25.8	13.78	0.96	22.70	Sbc	25.7	19.3	1.88	0.94	lo
										7.0	5.2	0.51	0.23	hi
L354P	11.96	0.97	18.05	0.56	23.4	14.54	0.87	23.35		4.9	3.7	0.24	0.36	lo
L355O	12.49	0.95	18.35	0.31	20.8	14.38	1.22	23.94	Sbc	6.0	4.5	0.49	0.39	lo
										15.1	11.3	1.24	0.97	hi
L359N	12.38	0.97	18.53	0.53	23.2					2.7	2.0	0.20		lo
L365O	12.81	1.25	18.69	0.17	22.8	16.83	0.10	25.68		2.9	2.2	0.32	1.77	lo
L374O	11.97	0.98	18.04	0.22	24.6	14.33	1.15	23.30	Sc	5.0	3.7	0.25	0.30	lo
L382P	12.50	1.59	18.28	0.64	21.4	17.42	0.35	24.02		2.2	1.6	0.18	2.27	lo
L385O	10.52	1.25	18.04	0.27	47.3	16.65	0.35	23.42	Sa	7.4	5.6	0.10	3.86	lo
(F25O)	12.27	1.14	19.05	0.38	20.1	15.64	1.02	24.48	Sd	6.5	4.9	0.43	1.33	lo
L411O	13.05	1.13	19.17	0.22	20.8	15.51	1.23	24.87		3.7	2.8	0.51	0.67	lo
L467O	12.38	1.24	18.34	0.23	25.6	13.93	1.33	23.22	Scd	3.4	2.5	0.25	0.14	lo
L493O	12.48	1.04	18.42	0.25	21.6	15.04	0.89	23.51	Sc	4.3	3.3	0.35	0.51	lo
L516O	12.07	0.99	18.79	0.40	34.0	14.75	0.84	23.40	Sbc	5.1	3.8	0.28	0.46	lo
										4.4	3.3	0.24	0.40	hi
L531O	12.31	1.25	18.02	0.22	20.8	15.13	0.92	23.95	Sc	2.8	2.1	0.20	0.36	lo
L536P	12.71	1.44	18.63	0.61	22.2	16.04	0.45	23.27		5.0	3.8	0.50	1.50	lo
L573P	12.64	1.08	18.60	0.18	24.8	15.47	1.26	24.85		2.8	2.1	0.26	0.49	lo
L574O	10.76	1.02	18.57	0.73	34.2	17.49	0.41	24.50		1.7	1.3	0.03	1.93	lo
L580N	10.81	1.49	19.39	0.64	38.6					1.6	1.2	0.03		lo
L589O	12.48	1.39	18.17	0.19	22.6	15.71	0.95	24.22	Scd	3.5	2.6	0.29	0.77	lo
L591O	12.73	1.27	18.79	0.76	21.6	15.42	0.88	23.93	Sbc	4.0	3.0	0.40	0.66	lo
L596O	11.67	0.85	18.47	0.31	36.0	14.25	1.22	23.44	SBbc	5.6	4.2	0.21	0.32	lo
L607O	11.84	0.94	18.13	0.67	21.8					2.8	2.1	0.13		lo
L616P	12.06	0.83	18.04	0.33	21.2	13.47	0.10			5.0	3.7	0.27	0.14	lo
F41O	12.42	0.79	18.47	0.48	14.3	15.64	0.84	24.05		4.3	3.2	0.33	0.88	lo
L621O	12.32	1.02	18.16	0.48	20.2	15.35	0.85	23.85	Sb	5.9	4.5	0.42	0.93	lo
L622O	12.11	1.02	18.01	0.54	21.0	15.15	0.10			3.4	2.5	0.19	0.44	lo
L630O	12.69	1.36	18.93	0.16	28.6	15.01	1.21	24.40	Sc	4.8	3.6	0.47	0.56	lo
F43N	13.73	0.97	18.76	0.45	13.0					4.1	3.1	1.05		lo
(L649P)	11.94	1.18	18.11	0.47	23.2		0.10			2.6	1.9	0.13		lo
L657N	12.53	1.18	18.32	0.22	21.6					1.5	1.1	0.13		lo
										3.7	2.8	0.31		hi
L666N	12.25	0.84	18.21	0.56	22.6					3.7	2.8	0.24		lo
L669O	12.33	1.16	18.11	0.28	20.2	15.10	0.90	23.61	Sbc	4.7	3.5	0.33	0.58	lo
L671N	12.85	1.15	18.64	0.16	20.6					8.3	6.2	0.95		lo
										6.9	5.2	0.79		hi
(L673O)	13.61	1.06	19.20	0.23	24.8	14.39	0.98	23.29	SBab	3.1	2.3	0.72	0.20	lo
L681P	12.05	0.97	18.06	0.47	21.0	15.52	0.74	23.66		3.5	2.6	0.19	0.64	lo
(F46N)	12.77	0.80	18.76	0.70	14.5					7.0	5.2	0.73		lo
L682O	12.69	1.24	18.49	0.25	21.2	15.59	0.89	24.00	Sc	4.0	3.0	0.40	0.79	lo
L686O	12.38	1.23	18.22	0.30	20.6	16.23	0.75	24.44		2.7	2.0	0.20	0.94	lo
(F48O)	12.95	1.12	19.06	0.78	9.1	16.52	0.61	24.22	S?	2.0	1.5	0.24	0.91	lo
L687O	12.66	1.14	18.45	0.17	24.0	15.06	1.06	23.86	Sc	3.5	2.6	0.33	0.42	lo
L689O	11.40	0.88	18.16	0.79	22.6	14.51	0.91	23.18	SBc	5.5	4.1	0.16	0.40	lo

Table 5b.3. Undetected objects – basic data - *continued*

No	K_{20} mag	$J - K$ mag	μ_{K5} $\frac{mag}{mas^2}$	b/a	$r_{K_{20}}$ ''	B_{T_c} mag	D_{25} '	$\mu_{B_{25}}$ $\frac{mag}{mas^2}$	T	rms mJy	I_{HI} $\frac{Jy km}{s}$	$\frac{M_{HI}}{L_K}$ solar units	$\frac{M_{HI}}{L_B}$	search mode
L691O	12.39	1.02	18.17	0.26	21.0	15.68	0.73	23.79	Sc	5.0	3.7	0.37	1.05	lo
L699O	11.81	1.00	18.06	0.50	22.8	14.83	0.97	23.61	Sab	6.1	4.6	0.27	0.59	lo
L706P	13.21	1.28	18.83	0.38	20.6	16.96	0.60	25.38		3.6	2.7	0.57	2.46	lo
L707N	11.84	1.03	19.07	0.18	48.4					2.4	1.8	0.11		lo
L708N	12.22	1.20	18.06	0.23	22.4					2.9	2.2	0.18		lo
L709P	11.15	1.17	18.11	0.42	40.0	13.62	0.48	23.71	Sc	2.0	1.5	0.05	0.06	lo
L733O	11.45	1.10	18.78	0.60	23.4					3.6	2.7	0.11		lo
L742O	11.88	1.01	18.04	0.55	21.2	14.10	0.81	23.02	SBc	4.4	3.3	0.20	0.22	lo
L744O	12.54	1.29	18.32	0.20	21.0	14.99	0.85	23.65	Sc	5.4	4.1	0.46	0.61	lo
L747O	12.23	0.90	18.46	0.29	24.6	13.95	1.08	23.05	Sc	10.2	7.6	0.66	0.43	lo
										9.0	6.8	0.58	0.36	hi
F51O	12.48	0.78	18.37	0.62	13.6	14.27	0.85	22.98	SBc	3.5	2.6	0.19	0.20	lo
L751N	11.77	0.99	18.76	0.41	21.6					2.4	1.8	0.10		lo
L753O	11.68	0.65	18.36	0.66	21.4	14.03	1.47	23.86	SBa	2.9	1.1	0.06	0.07	
L759P	11.51	0.94	18.12	0.69	24.0	14.07	1.05	23.19	Sc	5.1	3.8	0.17	0.25	lo
L760O	11.62	1.11	18.23	0.33	30.6	16.70	0.76	25.24		2.5	1.9	0.09	1.36	lo
L770O	12.47	1.19	18.25	0.22	21.2	15.13	1.08	23.99	Sbc	2.7	2.0	0.22	0.35	lo
L774O	12.19	0.99	18.17	0.42	21.2	14.78	0.87	23.95	Sc	4.0	3.0	0.25	0.37	lo
L775P	12.06	0.96	18.08	0.38	23.8	15.59	0.65	23.93		3.4	2.5	0.19	0.66	lo
(F55N)	13.75	0.97	19.26	0.70	15.3					2.1	1.6	0.55		lo
(L791O)	12.49	1.36	18.36	0.27	21.6	14.86	1.18	23.91	Sed	6.8	5.1	0.55	0.68	lo
L797O	12.28	1.12	18.29	0.20	25.0		0.97		Sc	3.0	2.3	0.20		lo
L819P	12.22	0.97	18.04	0.33	22.4	15.28	0.62	23.94		6.4	4.8	0.41	0.93	lo
(F59N)	12.50	1.01	18.83	0.52	16.7					4.9	3.7	0.40		lo
L836P	12.82	1.16	18.55	0.24	20.8	14.77	1.02	23.51	Sd	3.5	2.6	0.39	0.32	lo

Notes: two different H I line search modes were used: ‘lo’ in the -500 to $10,500$ km s $^{-1}$ range, and ‘hi’ in the $9,500$ to $20,500$ km s $^{-1}$ range. Estimated upper limits to I_{HI} and M_{HI} are 3σ values for 250 km s $^{-1}$ wide, flat-topped profiles.



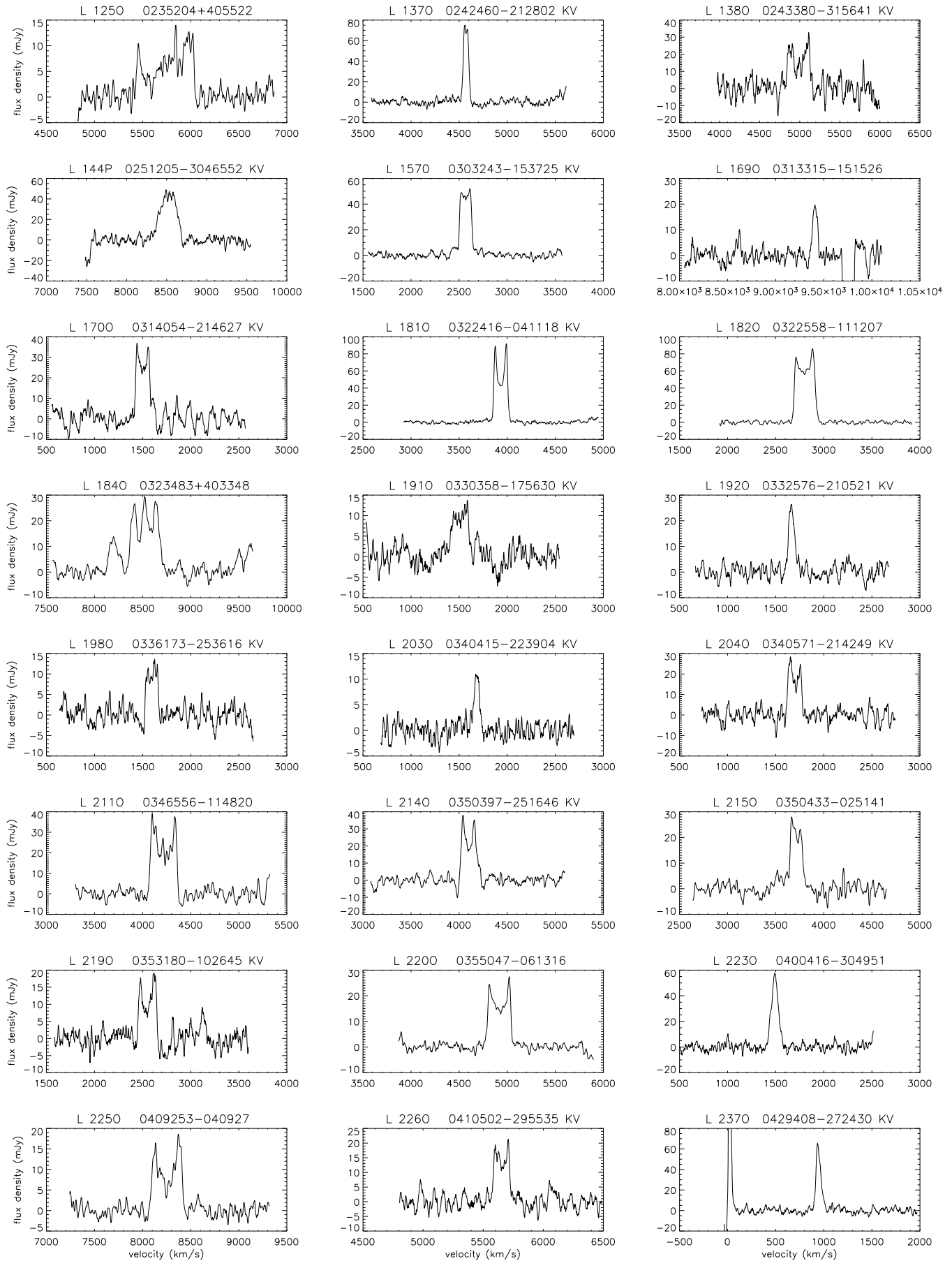


Fig. 1. b. Nançay 21-cm H I line spectra of detected objects - *continued*.

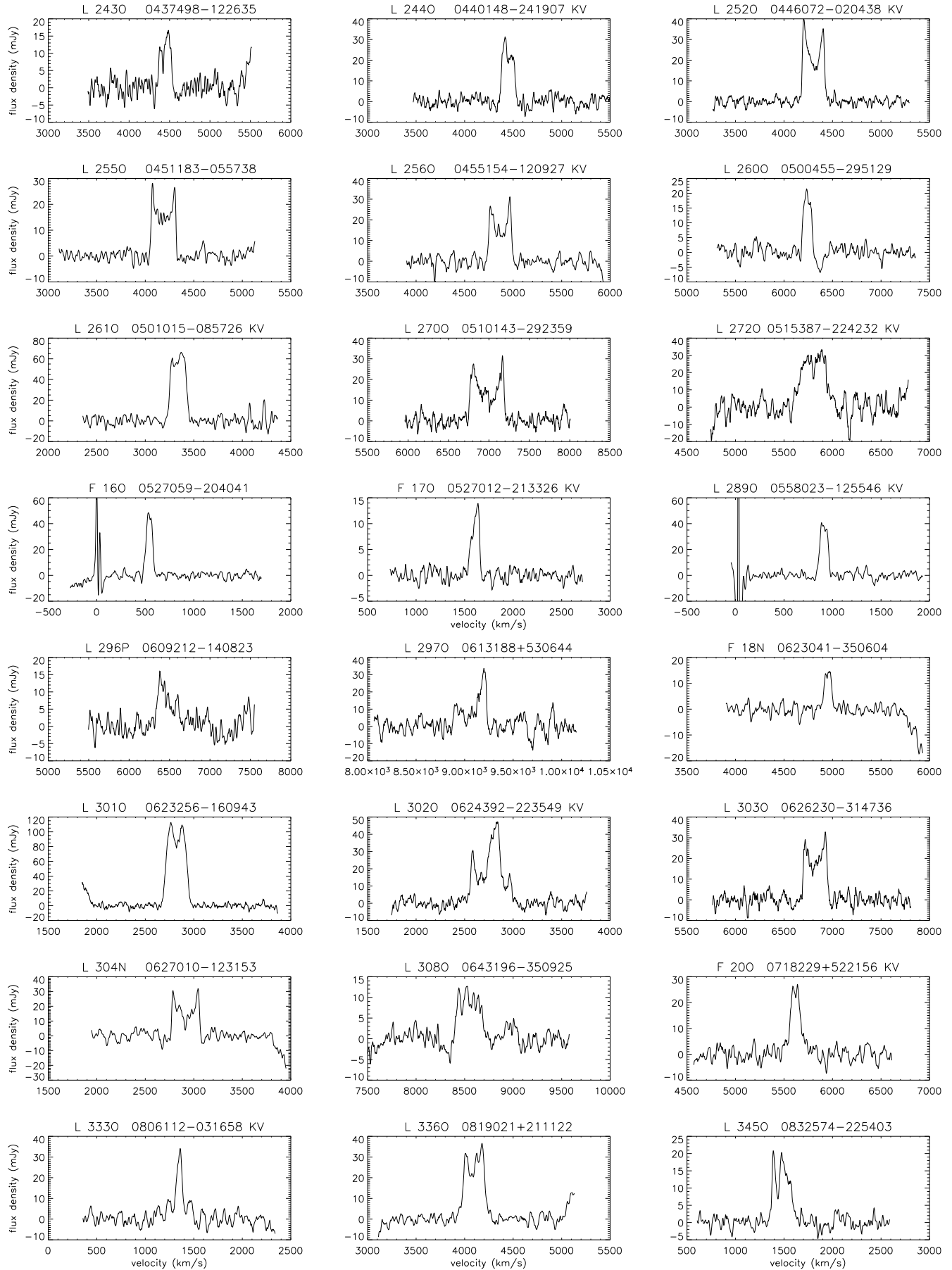


Fig. 1. c. Nançay 21-cm H I line spectra of detected objects - *continued*.

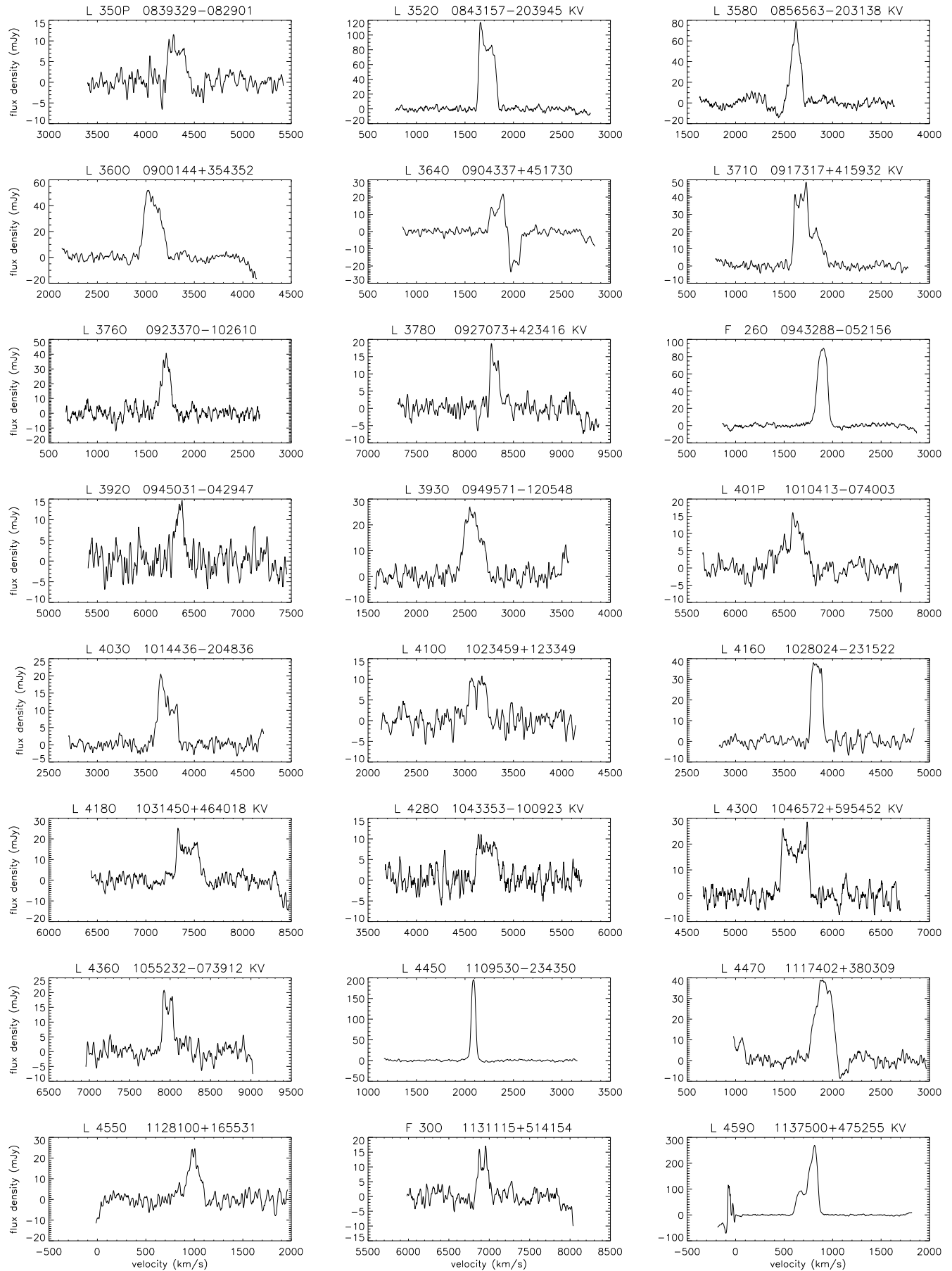


Fig. 1. d. Nançay 21-cm H I line spectra of detected objects - *continued*.

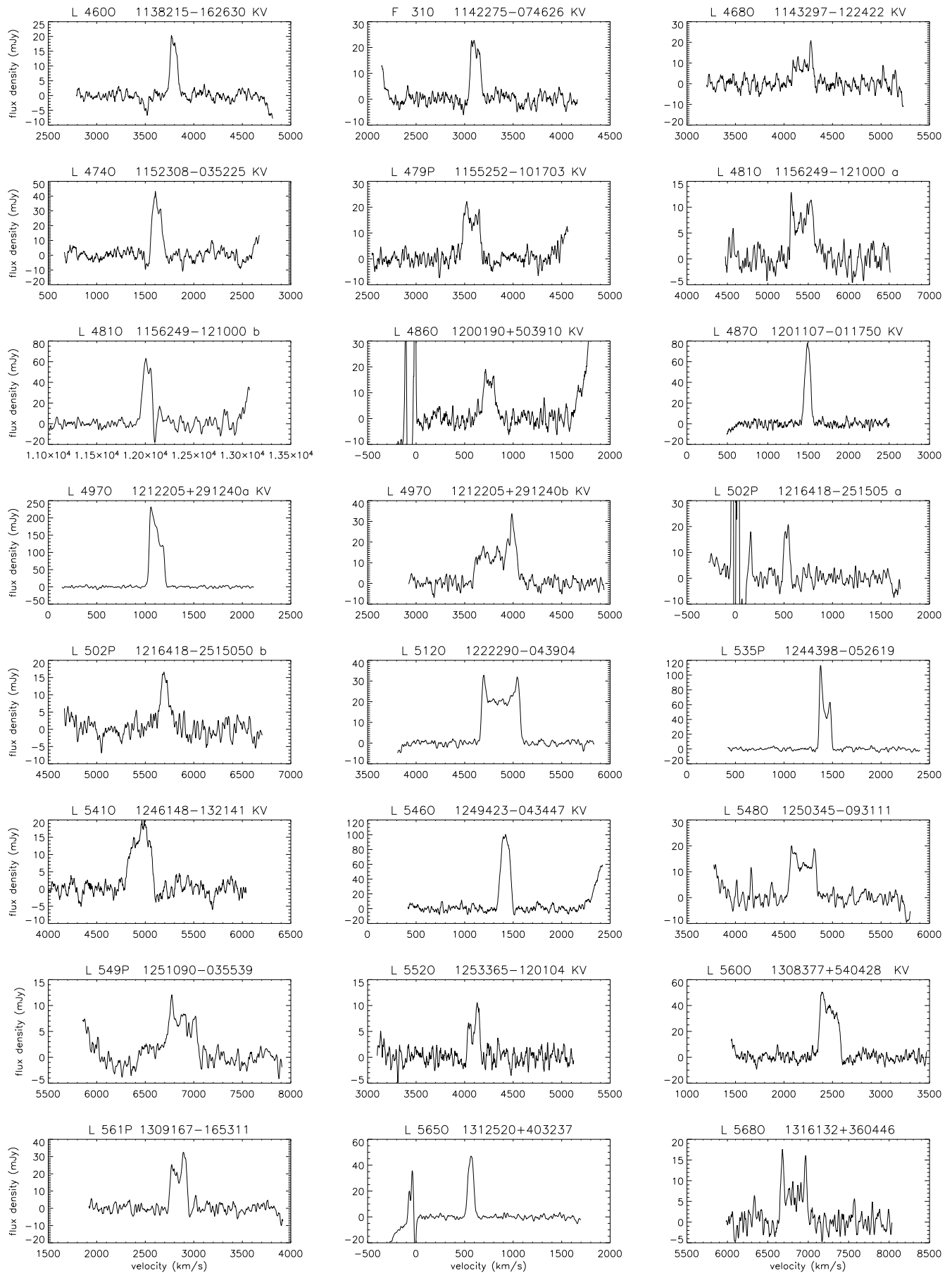


Fig. 1. e. Nançay 21-cm H I line spectra of detected objects - *continued*.

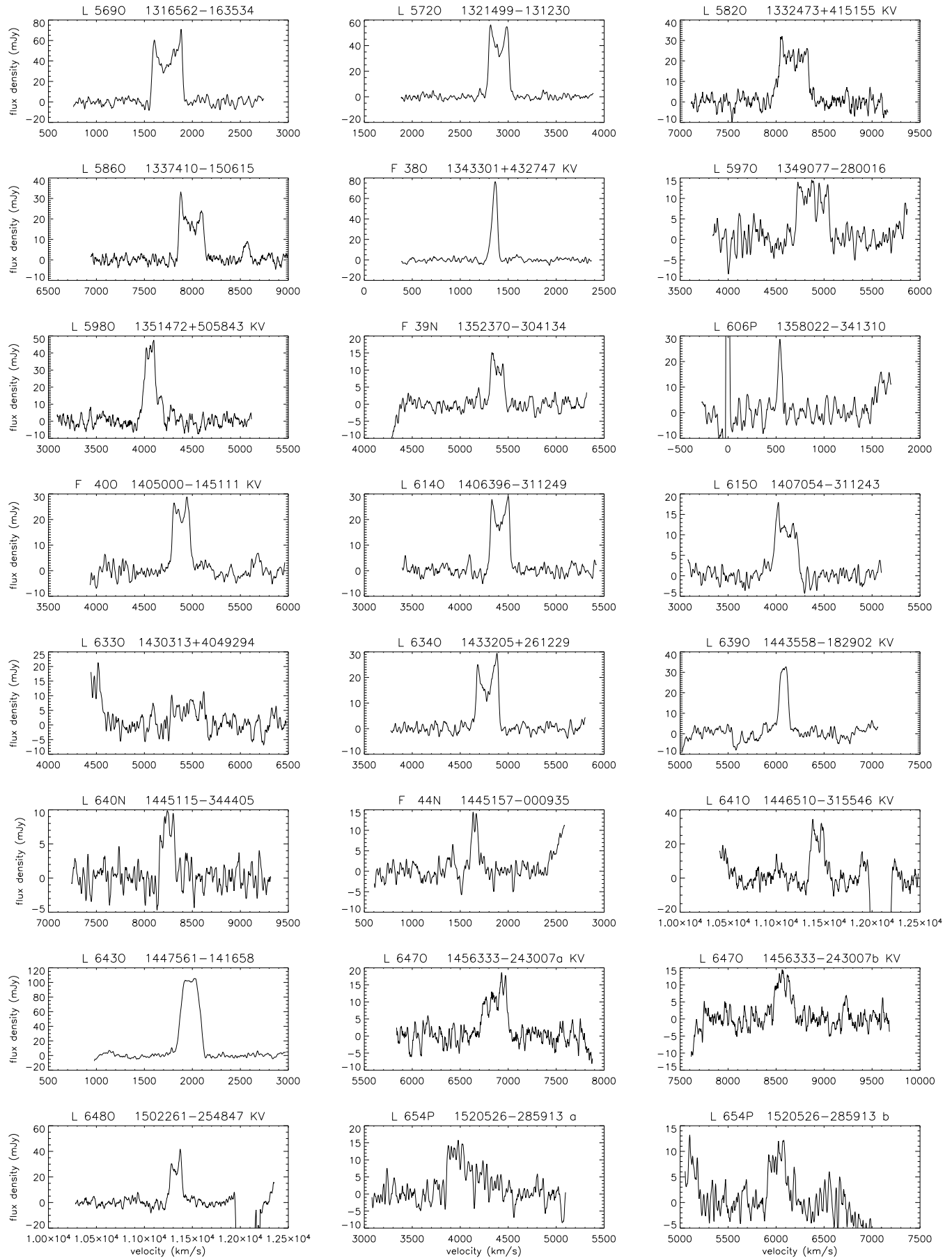


Fig. 1. f. Nançay 21-cm H I line spectra of detected objects - *continued*.

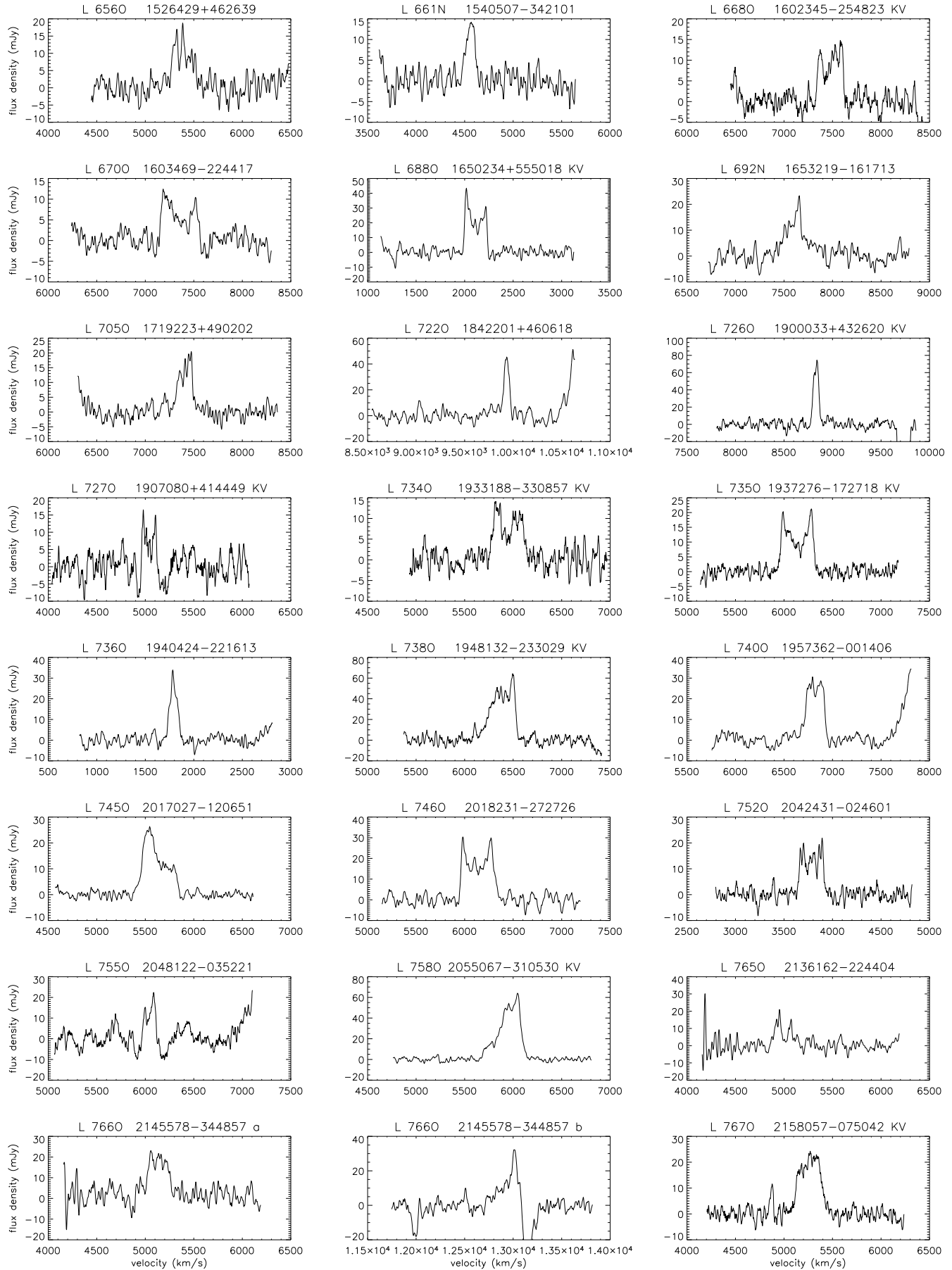
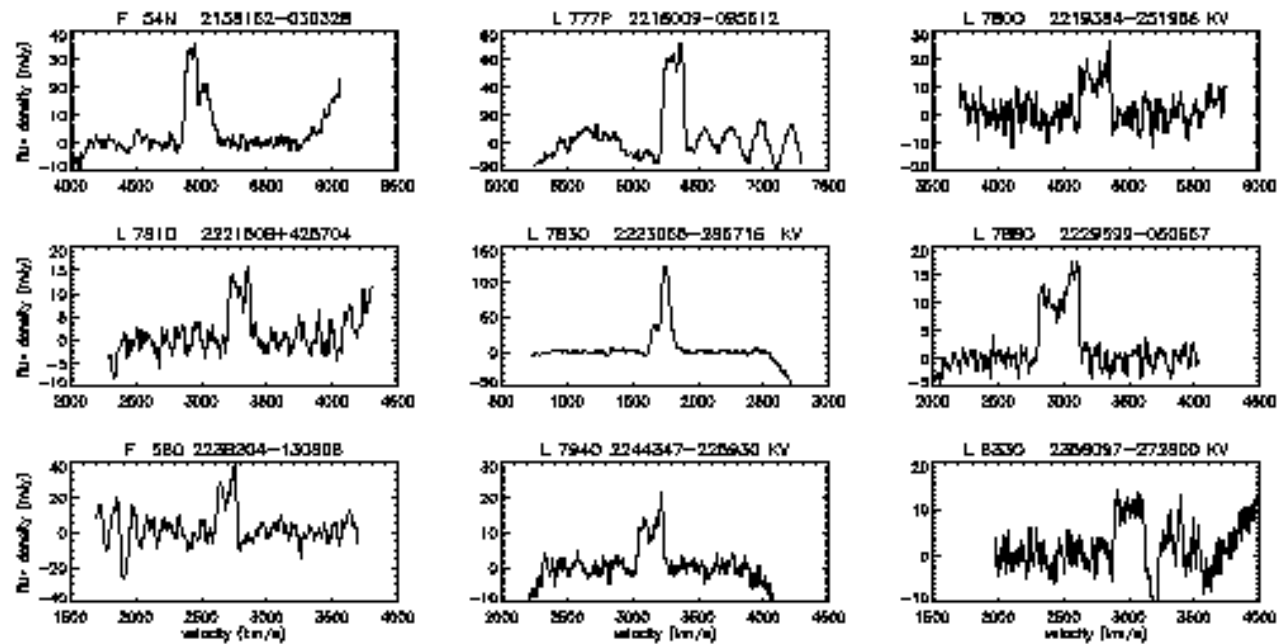


Fig. 1. g. Nançay 21-cm H I line spectra of detected objects - *continued*.



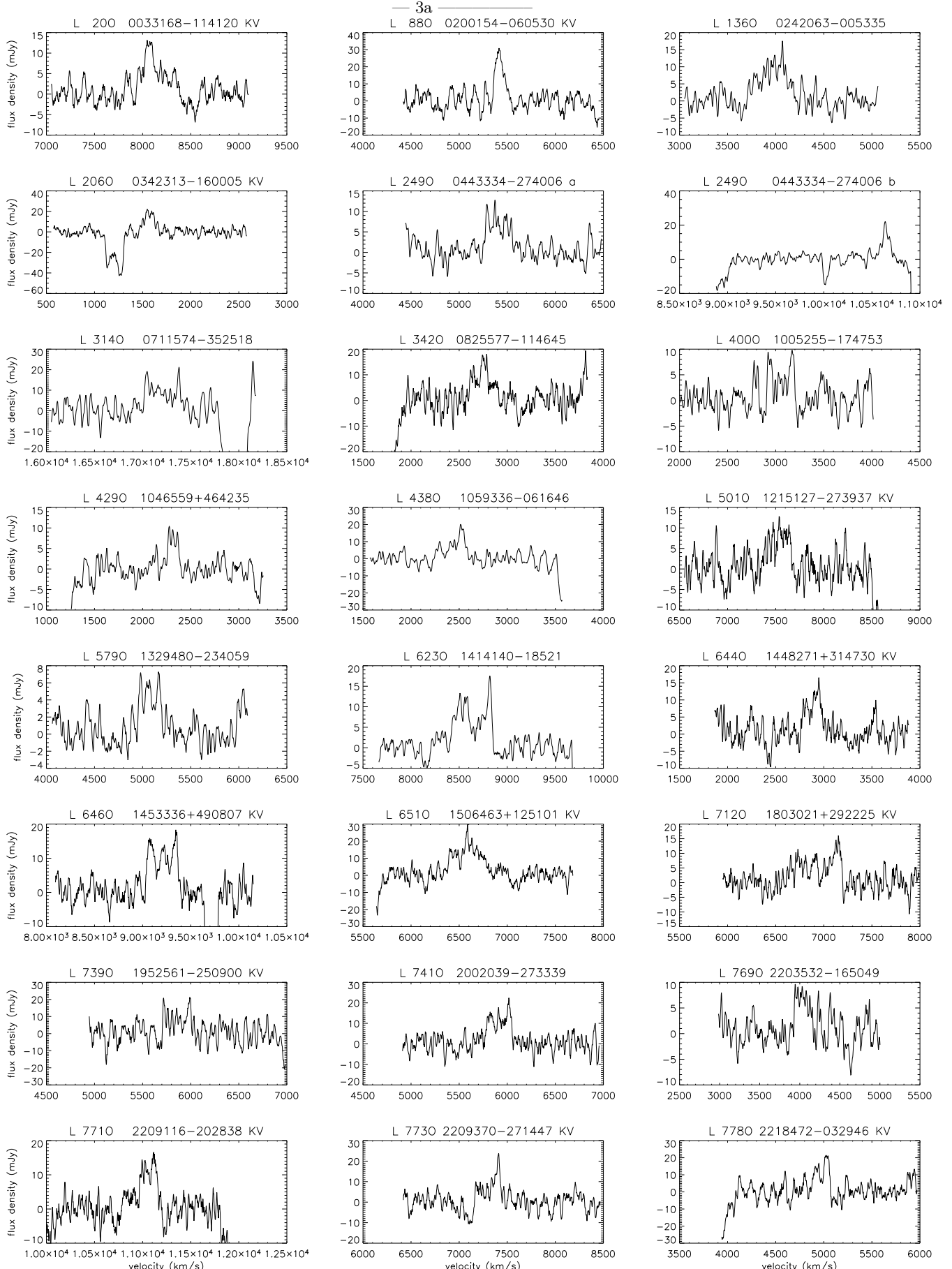


Fig. 2. a. Nançay 21-cm HI line spectra of marginal detections (see Table 4). Velocity resolution is 15.8 km s^{-1} (velocity search mode) and 17.1 km s^{-1} (known velocity mode), radial heliocentric velocities are according to the optical convention. Galaxies detected in the ‘known velocity’ mode are indicated by the designation ‘KV’ following their coordinates in the header of their spectrum.

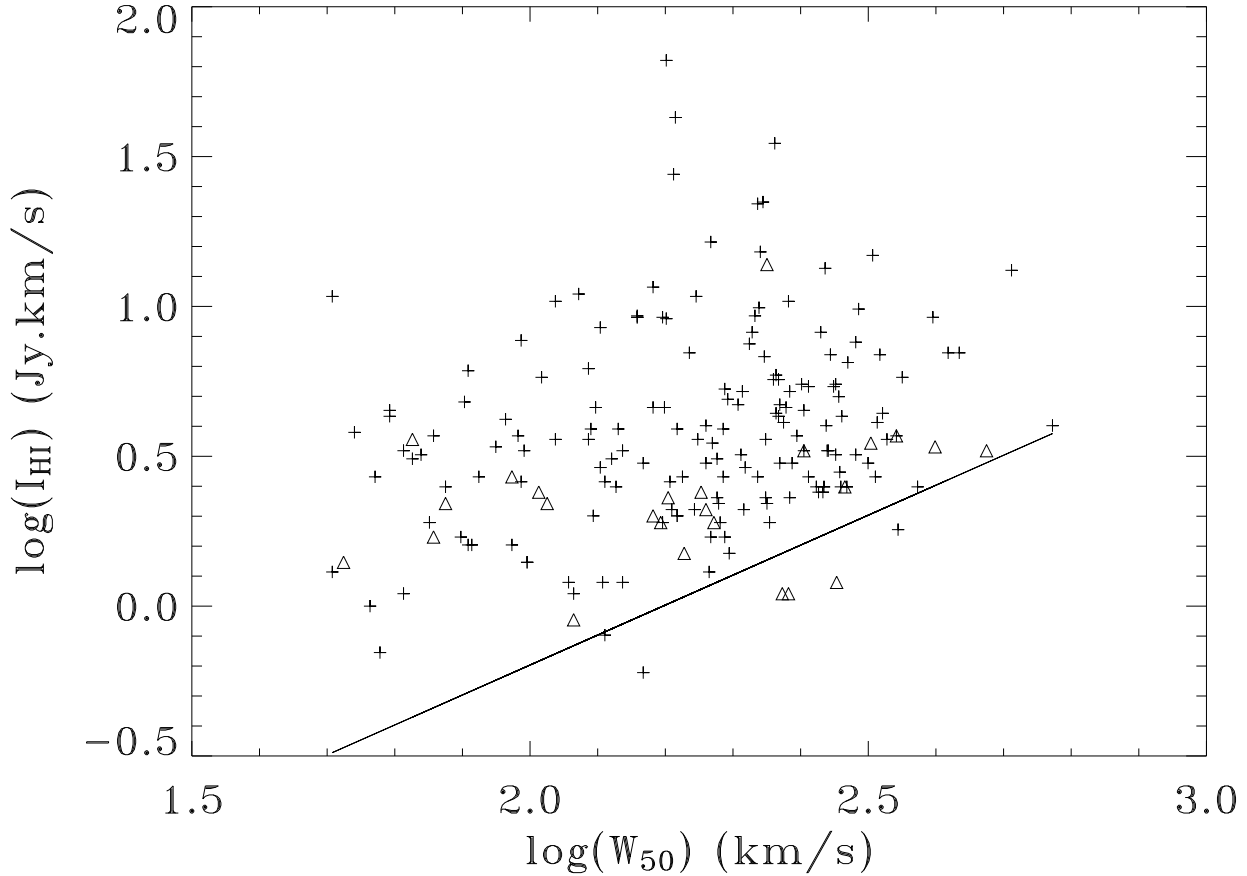


Fig. 3. Distribution of integrated H_I line fluxes I_{HI} as a function of the H_I line FWHM, W_{50} . The straight line indicates the 3 σ detection limit for a 250 km s⁻¹ wide, flat-topped spectral line, based on the average rms noise level of the data. Clear detections of survey galaxies are represented by crosses, and marginal detections by triangles.

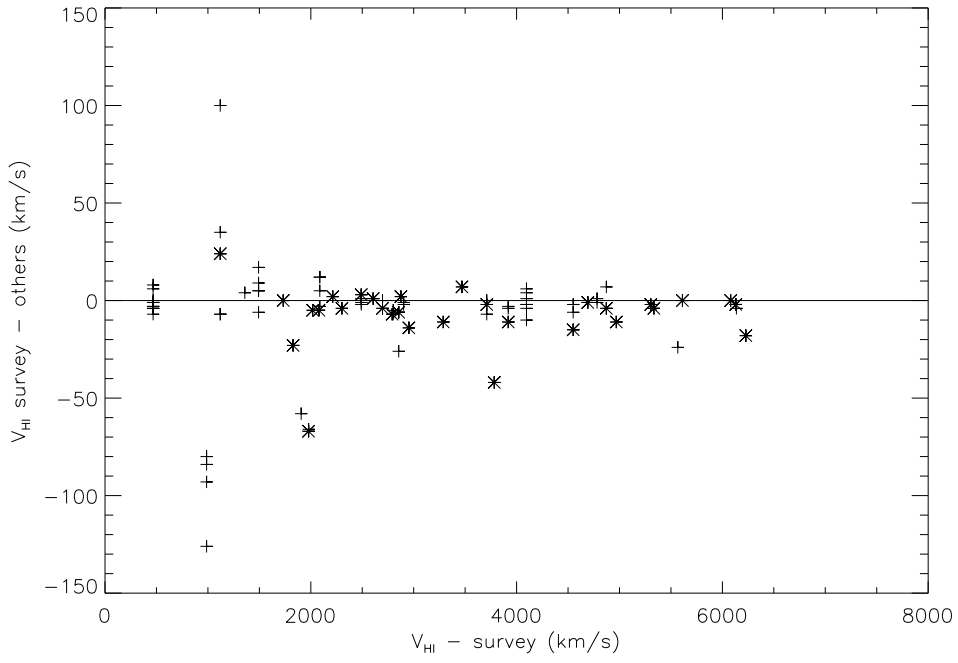


Fig. 4. Comparison of central H I profile velocities, V_{HI} , of survey and calibration galaxies with literature values (see Table 2). Plotted is the difference (survey-others) as function of the H I radial velocity measured in the survey. To guide the eye, a horizontal line was plotted at $\Delta V = 0 \text{ km s}^{-1}$; this line does not represent a fit to the data. Comparisons with published Nançay data are represented by a $*$, the crosses indicate comparisons to measurements made with other telescopes.

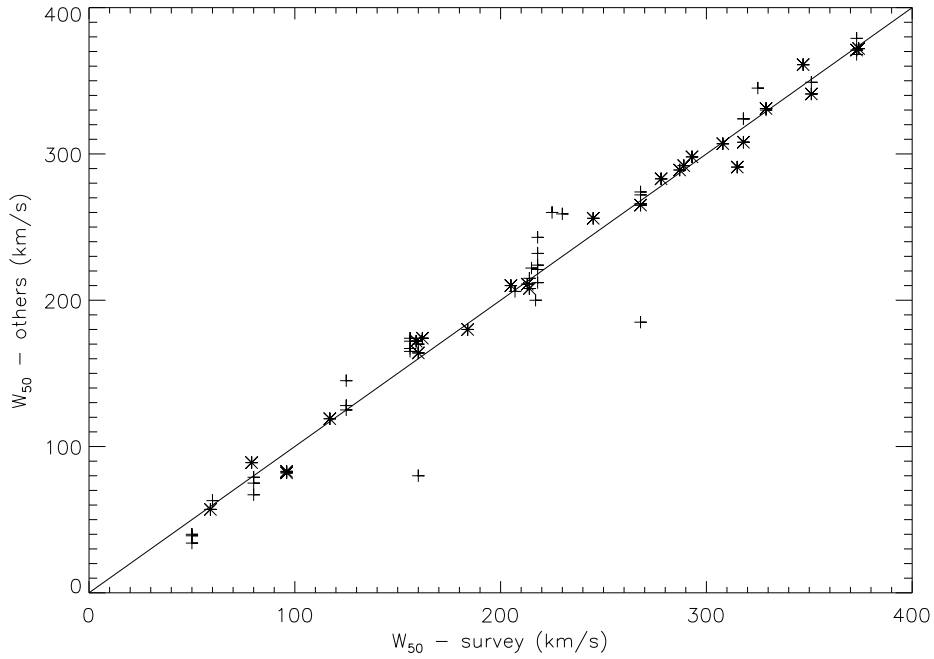


Fig. 5. Comparison of H I profile FWHMs, W_{50} , of survey and calibration galaxies with literature values (see Table 2). To guide the eye, a diagonal line with a slope of 1 was plotted; this line does not represent a fit to the data. Comparisons with published Nançay data are represented by a $*$, the crosses indicate comparisons to measurements made with other telescopes.

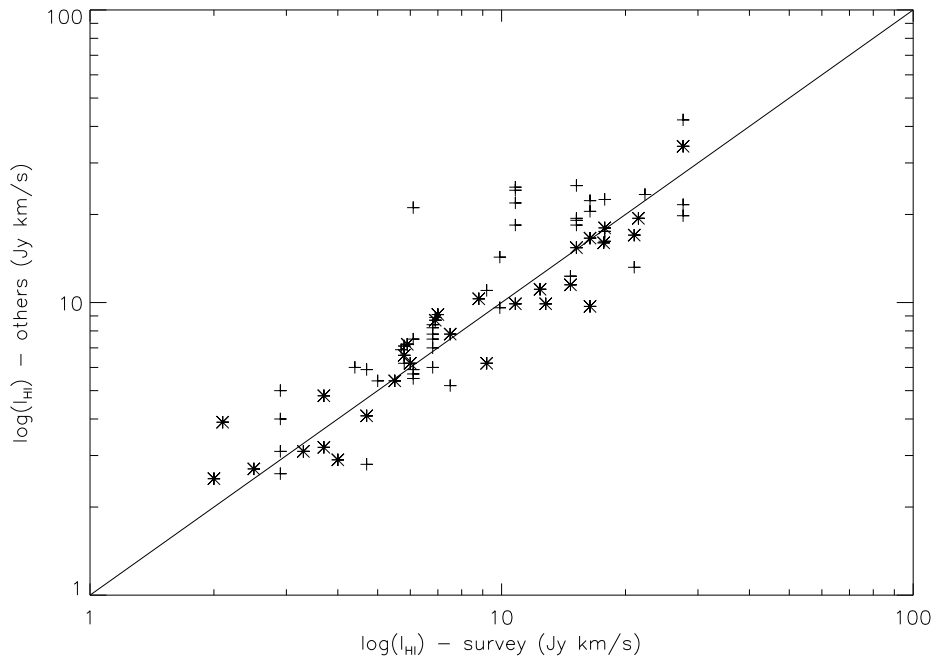


Fig. 6. Comparison of integrated H_I line fluxes, I_{HI} , of survey and calibration galaxies with literature values (see Table 2). To guide the eye, a diagonal line with a slope of 1 was plotted; this line does not represent a fit to the data. Comparisons with published Nançay data are represented by a \star , the crosses indicate comparisons to measurements made with other telescopes.